Plasticity in Structural and Functional Interactions between the Phosphoprotein and Nucleoprotein of Measles Virus

Yaoling Shu, Johnny Habchi, Stéphanie Costanzo, Andre Padilla, Joanna Brunel, Denis Gerlier, Michael Oglesbee, Sonia Longhi

THE JOURNAL OF BIOLOGICAL CHEMISTRY VOL. 287, NO. 15, pp. 11951–11967, April 6, 2012

Plasticity in Structural and Functional Interactions between the Phosphoprotein and Nucleoprotein of Measles Virus*[S]

Received for publication, December 16, 2011, and in revised form, February 7, 2012 Published, JBC Papers in Press, February 8, 2012, DOI 10.1074/jbc.M111.333088

Yaoling Shu[‡], Johnny Habchi[§], Stéphanie Costanzo[§], André Padilla[¶], Joanna Brunel[‖], Denis Gerlier[‖], Michael Oglesbee[‡1], and Sonia Longhi[§2]

From the [‡]Department of Veterinary Biosciences, Ohio State University, Columbus, Ohio 43210, the [§] Laboratoire d' Architecture et Fonction des Macromolécules Biologiques (AFMB), UMR 7257, CNRS, Aix-Marseille University, 163 Avenue de Luminy, Case 932, 13288 Marseille, France, the [¶]Centre de Biochimie Structurale, INSERM U554, UMR 5048, CNRS, University Montpellier 1 and 2, 29 rue de Navacelles, 34090 Montpellier, France, and the [‖]Laboratoire de Virologie Humaine, INSERM U758, Ecole Normale Supérieure de Lyon, University of Lyon 1, 69365 Lyon, France

Background: Binding of the MeV C-terminal disordered domain of the nucleoprotein (N_{TAIL}) to the X domain (XD) of the phosphoprotein mediates recruitment of the polymerase.
Results: N_{TAIL} amino acid substitutions that reduce N_{TAIL}-XD affinity and/or N_{TAIL} α-helical folding do not affect polymerase rates but strongly affect infectivity.
Conclusion: MeV polymerase tolerates N_{TAIL} amino acid substitutions.
Significance: N_{TAIL} sequence plays a role in optimal infectivity.

The measles virus (MeV) phosphoprotein (P) tethers the polymerase to the nucleocapsid template for transcription and genome replication. Binding of P to nucleocapsid is mediated by the X domain of P (XD) and a conserved sequence (Box-2) within the C-terminal domain of the nucleoprotein (N_{TAIL}). XD binding induces N_{TAIL} α-helical folding, which in turn has been proposed to stabilize the polymerase-nucleocapsid complex, with cycles of binding and release required for transcription and genome replication. The current work directly assessed the relationships among XD-induced N_{TAIL} folding, XD-N_{TAIL} binding affinity, and polymerase activity. Amino acid substitutions that abolished XD-induced N_{TAIL} α-helical folding were created within Box-2 of Edmonston MeV N_{TAIL}. Polymerase activity in minireplicons was maintained despite a 35-fold decrease in XD-N_{TAIL} binding affinity or reduction/loss of XD-induced N_{TAIL} alpha-helical folding. Recombinant infectious virus was recovered for all mutants, and transcriptase elongation rates remained within a 1.7-fold range of parent virus. Box-2 mutations did however impose a significant cost to infectivity, reflected in an increase in the amount of input genome required to match the infectivity of parent virus. Diminished infectivity could not be attributed to changes in virion protein composition or production of defective interfering particles, where changes from parent virus were within a 3-fold range. The results indicated that MeV polymerase activity, but not infectivity, tolerates amino acid changes in the XD-binding region of the nucleoprotein. Selectional pressure for conservation of the Box-2 sequence may thus reflect a role in assuring the fidelity of polymerase functions or the assembly of viral particles required for optimal infectivity.

Measles virus (MeV)[3] is a member of the Paramyxoviridae family within the Mononegavirales order. Mononegavirales are nonsegmented negative-stranded RNA viruses that share a complex and unique mode of transcription and replication (1, 2). Virions are enveloped, and the single strand of genomic RNA is encapsidated by the nucleoprotein (N). For MeV, the envelope contains hemagglutinin (H) and a fusion glycoprotein (F) that mediates tissue targeting and MeV entry (3–5). This process is coordinated by the matrix (M) protein, which also mediates packaging of nucleocapsid into virions by interacting with both glycoprotein tails and nucleoprotein (6). Nucleocapsids are filamentous, consisting of genomic RNA encapsidated into a regular helical array of N monomers. The structure of MeV N has been modeled (7) into the electron density of MeV nucleocapsids, using the crystal structure of the N protein from the respiratory syncytial virus as template (8). This ribonucleoprotein complex, rather than naked RNA, is the template for both transcription and replication. These latter activities are carried out by the RNA-dependent RNA polymerase that is composed of the large (L) protein and of the phosphoprotein (P). Once the viral ribonucleoprotein complexes are released into the cytoplasm of infected cells, the transcription of viral genes occurs using endogenous NTPs as substrate. Following primary transcription, the polymerase switches to a processive

* This work was supported, in whole or in part, by National Institutes of Health Grant R01 NS031693-11A2 from NINDS (to M. O.). This work was also supported by the CNRS and the Agence Nationale de la Recherche programs "Microbiologie et Immunologie" (ANR-05-MIIM-035-02) and "Physico-Chimie du Vivant" (ANR-08-PCVI-0020-01) (to D. G. and S. L.).
[S] This article contains supplemental Figs. S1 and S2 and Table S1.
[1] To whom correspondence may be addressed: Dept. of Veterinary Biosciences, Ohio State University, 1925 Coffey Rd., Columbus, OH 43210. Tel.: 614-292-9672; Fax: 614-292-6473; E-mail: michael.oglesbee@cvm.osu.edu.
[2] To whom correspondence may be addressed: AFMB, UMR 6098, 163 Ave. de Luminy, Case 932, 13288 Marseille, Cedex 09, France. Tel.: +33-91825580; Fax: +33-91266720; E-mail: Sonia.Longhi@afmb.univ-mrs.fr.

[3] The abbreviations used are: MeV, measles virus; N, nucleoprotein; F, fusion glycoprotein; M, matrix protein; H, hemagglutinin; L, large protein; P, phosphoprotein; N_{TAIL}, C-terminal disordered domain of N; XD, X domain of P; α-MoRE, molecular recognition element of α-helical nature; ITC, isothermal titration calorimetry; Ed, Edmonston strain of measles virus; TFE, 2,2,2-trifluoroethanol; CAT, chloramphenicol acetyltransferase; m.o.i., multiplicity of infection; h.p.i., hours post-infection.

mode and ignores the gene junctions to synthesize a full, complementary strand of genome length. This positive-stranded RNA (antigenome) does not serve as a template for transcription; its unique role is to provide an intermediate in genome replication. The intracellular concentration of the N protein is the main element controlling the relative level of transcription *versus* replication (9). When N is limiting, the polymerase functions preferentially as a transcriptase, thus leading to an increase in the intracellular concentration of viral proteins including N. When N levels are high enough to allow encapsidation of the nascent RNA chain, the polymerase functions preferentially as a replicase (see Refs. 10–12 for reviews on transcription and replication).

The L protein does not directly bind viral genomic RNA during transcription and genome replication but instead is tethered onto the viral ribonucleoprotein template via oligomers of P. As such, the P protein is an essential polymerase co-factor. The exact oligomeric state of MeV P is not known. By analogy with the closely related Sendai virus (13, 14), it is thought to be tetrameric, contrary to the dimeric P proteins of rabies and vesicular stomatitis viruses (15, 16). The P oligomers simultaneously bind to L (via the P multimerization domain) and to the exposed C-terminal domain of N (N_{TAIL}; amino acids 400–525) via the C-terminal X domain of P (XD; amino acids 459–507) (17–26). Progressive movement of the polymerase along its template thus is thought to require cycles of XD-N_{TAIL} binding and release (see Ref. 27 and references cited therein).

N_{TAIL} is an intrinsically disordered domain (12, 18) that undergoes α-helical folding upon binding to XD (17–26). Structure prediction and available experimental observations indicate that the disordered nature of the C-terminal region of N is a conserved feature within members of the Paramyxovirinae subfamily (29–32). Like all intrinsically disordered proteins (33–38), N_{TAIL} exists as a dynamic ensemble of interconverting conformers under physiological conditions of pH and salinity and in the absence of XD (24–26). Despite the overall paucity of N_{TAIL} in hydrophobic residues and the concomitant enrichment in polar and charged residues typical of intrinsically disordered proteins (39, 40), N_{TAIL} possesses two conserved hydrophobic patches: Box-2 (amino acids 489–506) and Box-3 (amino acids 517–525) (Fig. 1*A*). Box-2 contains a predicted molecular recognition element of α helical nature (α-MoRE), spanning residues 488–499 (18). MoREs are short, order-prone regions within intrinsically disordered regions that have a propensity to undergo induced folding (*i.e.* a disorder-to-order transition upon binding to a partner) (41–44). Several studies have confirmed the involvement of this α-MoRE in binding to XD, showing that the N_{TAIL} region encompassing residues 486–502 adopts an α-helical conformation when bound to XD (17–26, 45). The α-MoRE is partly preconfigured in solution prior to XD binding (21, 24–26), and binding to XD stabilizes the α-helical conformation, giving rise to a compact four-helix bundle in which the N_{TAIL}-XD interface is stabilized by hydrophobic contacts (17, 45). Binding of XD to Box-2 also induces a reduction in the conformational freedom of the downstream Box-3 region (21, 23, 25), likely reflecting the establishment of transient, nonspecific contacts between Box-3 and XD (24). Support for this model comes from two sources: (i) heteronuclear NMR studies showing magnetic perturbations in Box-3 associated with XD-N_{TAIL} binding (19, 24) and (ii) lack of a C-terminal appendage exposed to the solvent in the low resolution structural model of the XD-N_{TAIL} complex that was derived using small-angle x-ray scattering (19). These induced folding events have been proposed to stabilize the XD-N_{TAIL} complex (11, 46). The latter is characterized by an equilibrium dissociation constant (K_D) of ~100 nM, although the relationship between induced folding and binding affinity between N_{TAIL} and XD has not been directly tested.

A proposed link among induced folding, binding affinity, and polymerase function has been suggested by functional analysis of N_{TAIL} variants in the context of the full-length N protein (47). Strikingly, amino acids located C-terminally to Box-2 were found to impose constraint on viral polymerase function, as judged from minireplicon studies using N constructs with C-terminal truncations (47). Progressively larger deletions up to amino acid 501 result in progressively larger increases in minireplicon reporter gene expression, after which there is a precipitous loss of polymerase activity. These findings, combined with the observed loss of conformational freedom of Box-3 upon binding to XD, support the view that XD-induced structural changes in N_{TAIL} select for Box-3 conformers, stabilizing the XD-N_{TAIL} complex. In turn, stability of the N_{TAIL}-XD complex (measured by the XD-N_{TAIL} binding affinity) would impose constraint on the cycles of binding and release that are required for the polymerase to move along the template. Understanding these structure-function relationships will be essential in defining the mechanistic basis by which host and viral factors may enhance polymerase function.

The objective of the present study was to establish directly the relationships among XD-induced N_{TAIL} folding, complex stability, and polymerase activity. The hypothesis tested was that XD-induced N_{TAIL} folding maintains XD-N_{TAIL} binding affinity, which in turn regulates polymerase activity. Our approach was to create amino acid substitutions in the Box-2 helix-forming region that would reduce XD binding affinity and/or XD-induced conformational changes. Taking into account the fact that the N_{TAIL}-XD interface is dominated by hydrophobic contacts, we introduced charged (*i.e.* acidic) amino acids within Box-2 without however replacing large hydrophobic residues that might be essential for the XD-N_{TAIL} interaction. The side chains of the introduced residues were of a size comparable to that of the native side chain. Two N_{TAIL} variants were created in which the acidic group was oriented slightly toward the interface between XD and the N α-helix encompassing residues 486–502 (Q499E and A502D), and one was created in which the acidic side group faced away from the interface (A500D) (Fig. 1, *B* and *C*). Two of these substitutions also lie within the region of Box-2 that is essential for polymerase function in minireplicons (*i.e.* they are located upstream amino acid 501), and one lies C-terminally to this region, targeting amino acids that dampen viral polymerase activity. The binding affinity of the N_{TAIL} variants for XD was measured using isothermal titration calorimetry (ITC) to achieve reliable data for potentially low affinity interactions. In addition, the impact of these mutations on the biophysical properties of N_{TAIL} was established, including the propensity for α-helix for-

mation. The ability of the mutated N proteins to support viral polymerase function was tested in MeV minireplicons. The recombinant infectious Edmonston-based strain of MeV (Ed) was used to characterize the effect of the mutations on the level and kinetics of viral transcript and genome production.

EXPERIMENTAL PROCEDURES

Generation of N_{TAIL} Constructs and Purification of N_{TAIL} Proteins—Coding regions for all N_{TAIL} constructs were obtained by PCR using as template the plasmid pDEST14/$N_{TAIL\text{-}HN}$, which encodes residues 401–525 of the Ed MeV N protein with an N-terminal hexahistidine tag (19). Each mutant construct was obtained using Turbo-*Pfu* polymerase (Stratagene) and a pair of complementary mutagenic primers (Invitrogen). After digestion of the PCR mixture with DpnI to remove the methylated DNA template, *Escherichia coli* was transformed with the amplified PCR product. The sequence of the primers used to generate the N_{TAIL} Q499E, N_{TAIL} A500D, N_{TAIL} A502D, and N_{TAIL} G503D coding constructs is provided in supplemental Table S1. *E. coli* strain DH5α (Stratagene) was used for selection and amplification of DNA constructs. Bidirectional sequence analysis of the coding region of all expression plasmids was performed (MilleGen).

The *E. coli* strain Rosetta (DE3)pLysS (Novagen) was used for expression of recombinant proteins. Because the MeV N gene contains several rare codons that are used with a very low frequency in *E. coli*, co-expression of N_{TAIL} constructs with the plasmid pLysS (Novagen) was carried out. This plasmid, which supplies six rare tRNAs, also carries the lysozyme gene, thus allowing tight regulation of the expression of the recombinant gene as well as facilitating lysis. Cultures were grown overnight to saturation in Luria-Bertani (LB) medium containing 100 μg/ml ampicillin and 34 μg/ml chloramphenicol. An aliquot of the overnight culture was diluted 1/25 in LB medium and grown at 37 °C. When absorbance at 600 nm (A_{600}) reached 0.6–0.8, isopropyl β-D-thiogalactopyranoside was added to a final concentration of 0.2 mM, and the cells were grown at 37 °C for an additional 3 h. The induced cells were harvested, washed, and collected by centrifugation (5000 × *g*, 10 min). The resulting pellets were frozen at −20 °C.

The N_{TAIL} proteins were purified to homogeneity (>95%) from the soluble fraction of bacterial lysates in two steps: immobilized metal affinity chromatography (IMAC) and size exclusion chromatography (SEC). Cellular pellets of bacteria transformed with the different N_{TAIL} expression plasmids were disrupted by sonication in 5 volumes (v/w) of buffer A (50 mM sodium phosphate, pH 8, 300 mM NaCl, 10 mM imidazole, and 1 mM phenylmethylsulfonyl fluoride (PMSF)) supplemented with lysozyme (0.1 mg/ml), DNase I (10 μg/ml), 20 mM $MgSO_4$, and protease inhibitor mixture (Sigma; 50 μl/g cells). The lysate was clarified by centrifugation at 30,000 × *g* for 30 min. The clarified supernatant, as obtained from a 1-liter culture, was incubated for 1 h with 4 ml of chelating Sepharose Fast Flow resin preloaded with Ni^{2+} ions (GE Healthcare) equilibrated previously in buffer A. The resin was washed with buffer A containing 20 mM imidazole, and the N_{TAIL} proteins were eluted in buffer A containing 250 mM imidazole. Eluates were analyzed by SDS-PAGE. Fractions containing the recombinant product were concentrated using centrifugal filtration (Centricon Plus-20, 5000-Da molecular cutoff, Millipore). The proteins were then loaded onto a S200 HR 10/30 column (GE Healthcare) and eluted in 10 mM sodium phosphate, pH 8.

The apparent molecular mass values of proteins were based on elution profiles from gel filtration columns using low molecular weight and high molecular weight calibration kits (LMW/HMW, GE Healthcare). The theoretical Stokes radii (R_S) of a native (R_SN) and fully unfolded (R_SU) protein were calculated according to $\log(R_SN) = 0.369\log(MM) - 0.254$ and $\log(R_SU) = 0.533\log(MM) - 0.682$, with MM being the molecular mass (in Daltons) and R_S being expressed in Å.

Purification of histidine-tagged XD has been described previously (19). Protein concentrations were calculated by using either the theoretical absorption coefficients ϵ(mg $ml^{-1}\cdot cm^{-1}$) at 280 nm as obtained using the program ProtParam at the ExPASy server or the Bio-Rad protein assay reagent (Bio-Rad).

Dynamic Light Scattering—Dynamic light scattering experiments were performed with a Zetasizer Nano-S (Malvern) at 20 °C. Protein samples were diluted in 10 mM sodium phosphate buffer, pH 7, to a final concentration of 170 μM (N_{TAIL} A502D) or 2.4 mM (XD). The samples were filtered prior to taking the measurements (Millex syringe filters, 0.22 mm, Millipore). Diffusion coefficients were inferred from the analysis of the decay of the scattered intensity autocorrelation function. All calculations were performed using the software provided by the manufacturer.

Isothermal Titration Calorimetry—ITC experiments were carried out either on a VP-ITC or on an ITC 200 isothermal titration calorimeter (Microcal, Northampton, MA) at 20 °C. Protein pairs used in the binding analyses were dialyzed against 10 mM sodium phosphate, pH 7.0, 1 mM PMSF, and 0.02% sodium azide to minimize undesirable buffer-related effects. The dialysis buffer was used in all preliminary equilibration and washing steps. The same XD sample was used in all binding reactions. When the VP-ITC device was used, the concentration of N_{TAIL} proteins was initially adjusted to 9–12 μM in the microcalorimeter cell (1.41 ml), and a 10-μl volume of XD (stock solution at 150 μM) was added from a computer-controlled 300-μl microsyringe at 5-min intervals. In the case of binding reactions to parent N_{TAIL} and N_{TAIL} Q499E, N_{TAIL} was also used as the injectant (from a stock at 145–155 μM), added progressively to XD (at 12–14 μM).

For experiments carried out on the ITC 200 device, the concentration of parent NTAIL and A500D N_{TAIL} proteins was initially adjusted to 20 μM in the microcalorimeter cell (0.2 ml), and XD (stock solution at 200 μM) was added from a computer-controlled 40-μl microsyringe via a total of 19 injections of 2 μl each at intervals of 180 s. For the N_{TAIL} A502D-XD couple, numerous experiments were carried out in which XD at various concentrations (from 200 μM up to 2.4 mM) was added progressively in the microcalorimeter cell in which the concentration of the N_{TAIL} variant ranged from 20 to 200 μM. Heat dilution of the ligand was taken into account from peaks measured after full saturation of the protein sample contained in the microcalorimeter cell by the ligand.

A theoretical titration curve was fitted to the experimental data using the Origin software (Microcal). This software uses

the relationship between the heat generated by each injection and ΔH° (enthalpy change in cal mol^{-1}), K_a (association binding constant in M^{-1}), n (number of binding sites per monomer), total protein concentration, and free and total ligand concentrations. The variation in the entropy (ΔS in cal mol^{-1} deg^{-1}) of each binding reaction was inferred from the variation in the free energy (ΔG), where this latter was calculated from the following relation: $\Delta G = -RT\ln 1/K_a$.

Circular Dichroism (CD)—Structural variations of N_{TAIL} proteins were measured as a function of changes in the initial far-UV CD spectrum following the addition of either increasing concentrations of 2,2,2-trifluoroethanol (TFE) (Sigma-Aldrich) or a 2-fold molar excess of XD or lysozyme (Sigma-Aldrich), where this latter served as a negative control. The CD spectra were recorded on a Jasco 810 dichrograph using 1-mm-thick quartz cells in 10 mM sodium phosphate, pH 7, at 20 °C. CD spectra, measured between 185 and 260 nm at 0.2 nm/min, were averaged from three independent acquisitions. Mean ellipticity values per residue ([Θ]) were calculated as $[\Theta] = 3300 m\Delta A/(lcn)$, where l (path length) = 0.1 cm, n = number of residues, m = molecular mass in daltons, and c = protein concentration expressed in mg/ml. Number of residues (n) is 132 for N_{TAIL} variants, 56 for XD, and 129 for lysozyme, and m values are 14,676 Da for N_{TAIL} variants, 6,690 Da for XD, and 14,300 Da for lysozyme. Protein concentrations of 0.1 mg/ml were used when recording the spectra of both individual and protein mixtures. In the case of protein mixtures, mean ellipticity values per residue ([Θ]) were calculated as $[\Theta] = 3300 \Delta A/\{[(C_1 n_1)/m_1) + (C_2\, n_2/m_2)]l\}$, where l (path length) = 0.1 cm, n_1 or n_2 = number of residues, m_1 or m_2 = molecular mass in daltons, and c_1 or c_2 = protein concentration expressed in mg/ml for each of the two proteins in the mixture. The theoretical average ellipticity values per residue ($[\Theta]_{avg}$), assuming that neither disorder-to-order transitions nor secondary structure rearrangements occur, were calculated as follows: $[\Theta]_{avg} = [([\Theta]_1 n_1) + ([\Theta]_2 n_2 R)]/(n_1 + n_2 R)$, where $[\Theta]_1$ and $[\Theta]_2$ correspond to the measured mean ellipticity values per residue, n_1 and n_2 to the number of residues for each of the two proteins, and R to the excess molar ratio of protein 2.

The simulated CD spectrum of a mixture containing a 2-fold molar excess of XD and in which only 15% of N_{TAIL} binds to XD was generated. First, the CD spectrum of "folded" N_{TAIL} was obtained from the CD spectrum (in millidegrees) of a mixture containing native N_{TAIL} and XD in a 1:2 molar ratio upon subtraction of the XD contribution. Then, the CD spectrum of a mixture containing 15% folded N_{TAIL} and 85% unfolded (*i.e.* unbound) N_{TAIL} was obtained by summing up the spectrum of folded N_{TAIL} multiplied by 0.15 and the spectrum of unfolded (*i.e.* free) N_{TAIL} multiplied by 0.85. Finally, this latter spectrum was summed up to the spectrum of XD, and the mean ellipticity values per residue were calculated as described above.

The experimental data in the 185–260-nm range were analyzed using the DICHROWEB website, supported by grants to the Biotechnology and Biological Sciences Research Council Centre (BBSRC) for Protein and Membrane Structure and Dynamics (48, 49). The CDSSTR deconvolution method was used to estimate the content of the α-helical and disordered structures using as reference the protein set 7.

N Protein Mutagenesis and Minireplicon Reporter Gene Expression—Oligonucleotide-mediated site-directed mutagenesis of a MeV N gene cDNA (pT7MV-N expression plasmid) was performed as described previously (47). In brief, *dut ung* mutant *E. coli* RZ1032 was used to generate single-stranded pT7MV-N, which contains uracil instead of thymidine. Mutagenic oligonucleotide primers were then annealed to the single-stranded pT7MV-N, extended, and ligated *in vitro*, and the double-stranded plasmid with desired Box-2 mutations was used to transform *E. coli* DH5α. To facilitate the identification of the desired Box-2 mutations, mutagenic primers were designed to also incorporate nucleotide substitutions that did not affect coding but added or eliminated a unique restriction endonuclease site. The sequence of the primers used to generate the mutated N constructs is provided in supplemental Table S1. After the plasmids were screened by restriction endonuclease digestion, the inserts were sequenced bidirectionally to confirm the presence of desired Box-2 mutations and to rule out the presence of second site mutations. Resultant pT7-MV-N plasmids carrying the Box-2 mutations were tested for their ability to support MeV minireplicon reporter gene expression.

Minireplicon experiments were performed as described previously (47). Briefly, HEp-2 cells were cultured in 6-well plates at 37 °C, 5% CO_2, in minimum essential medium containing Earle's salts (1× MEM) and 10% fetal bovine serum. Calcium phosphate transfection of subconfluent monolayers was used to simultaneously introduce three plasmids that encode MeV N (0.8 μg of pT7MV-N, pT7MV-N Q499E, pT7MV-N A500D, or pT7MV-N A502D), P (0.6 μg of pT7MV-P), and L (0.2 μg of pT7MV-L) proteins and one plasmid expressing MeV minigenomic RNA (0.2 μg of pMV107-CAT). The minigenome contained MeV genomic termini flanking the chloramphenicol acetyltransferase (CAT) coding sequence. Expression was driven by T7 polymerase encoded by a replication-deficient recombinant vaccinia virus MVAT7, introduced at a multiplicity of infection (m.o.i.) of 2. In addition, a T7-mediated luciferase expression vector (0.2 μg of pT7-GL3-Luc) was included as a control for transfection efficiency.

Cells were harvested at 30 h post-transfection into 250 μl of reporter lysis buffer. Twenty μl of cell lysate was added to a luciferase assay system (Promega) and fluorescence recorded on a PerkinElmer LS-5B luminescence spectrometer. Fifty μl of cell lysate was analyzed for CAT activity using a FAST CAT yellow (deoxy)chloramphenicol acetyltransferase assay kit (Molecular Probes Inc., Eugene, OR). CAT reaction products were resolved using silica gel thin layer chromatography, and the UV fluorescence intensity was quantified using an AlphaImager 2000 documentation and analysis system (AlphaEase software). Luciferase activity was used to normalize the CAT data.

Generation and Characterization of Recombinant Infectious Ed MeV Incorporating Box-2 Mutations—Recombinant MeV encoding N protein Box-2 mutations were generated and rescued using previously described methods (51). Oligonucleotide site-directed mutagenesis (QuikChange II XL site-directed mutagenesis kit, catalog No. 200523) was performed on a 2310-bp subclone of the full-length MeV genomic cDNA, with

this latter contained in plasmid p+MV (52). The subclone included the complete N gene and 239 bp of the 5′ P gene coding region. The sequence of the primers used to generate the mutated MeV N subclones is provided in supplemental Table S1. To generate a full-length genomic cDNA containing the Box-2 mutations, p+MV and the genome cDNA subclones were digested with SfiI and SacII. The purified 2310-bp subclone was sequenced to rule out the presence of spurious second site mutations and then ligated into the 16,631-bp parent genomic cDNA. Resultant full-length MeV genome plasmids with Box-2 mutations (p+MV-N Q499E, p+MV-N A500D, or p+MV-N A502D) were amplified in XL10-Gold ultracompetent cells (Stratagene). Purified plasmids containing the desired mutations were identified by their unique restriction enzyme digestion patterns as described above for N. Infectious virus was rescued from Hep-2 cells as described previously (51). Cells were transfected with plasmids expressing plus sense MeV genomic RNA, and Ed N, P, and L messenger RNAs. T7 was provided by MVAT7. Viruses containing the Box-2 mutations were rescued on Vero cells in parallel with the parental virus (Ed N, derived from p+MV), plaque-purified, and used to generate low passage pools. Sequence analysis of genomic RNA from these viral pools confirmed the presence of the desired C-terminal N gene mutation.

Multistep growth curves for the recombinant viruses were established on subconfluent Vero cell monolayers in 6-well plates (m.o.i. = 0.01). Infection with each virus was performed in triplicate, and 1 ml of culture supernatant was collected at 12-h intervals between 24 and 72 h post-infection (h.p.i.). Progeny were titrated on Vero cells, reported as the 50% tissue culture infective dose ($TCID_{50}$)/ml. Cell-free virus for Ed N MeV and each of the three Box-2 mutants was purified from the supernatant of virus-infected Vero cells at 48 h.p.i. by sedimentation on a discontinuous sucrose gradient. Sucrose gradient-purified viruses were characterized by SYBR Green real time RT-PCR analysis of the L-trailer/F genome ratio as a measure of defective interfering particle content (9, 53).

Virion N, P, M, and F protein composition was also quantified by dot blot analysis according to a previously described procedure (54). Briefly, serial 2-fold dilutions of purified virus in 200 μl of phosphate-buffered saline were adsorbed onto a nitrocellulose sheet using a 96-well manifold and vacuum aspiration. After drying, the membrane was incubated in 50 mM Tris-HCl buffer, pH 7.5, and 150 mM NaCl containing 5% fat-free milk powder and 2% Tween 20 to permeabilize the virions. Then, the membrane was probed sequentially with mouse monoclonal antibodies against the viral proteins followed by incubation with a peroxidase-conjugated anti-Ig antibody. The signal was captured using luminescence imaging of each spot and quantified by ImageQuant (Bio-Rad). The signal from serial dilutions of virus was used to calculate the relative viral protein content from the linear part of the titration curve, expressed as log(1/volume) as a function of log(luminescence) in arbitrary units. Results were expressed as the percentage of parental Ed virus titer values.

Viral mRNA and genome production was defined by Northern blot analysis of total cell RNA to assess the integrity of viral transcript and genome production and by SYBR Green real-time RT-PCR analysis to assess the kinetics of viral RNA production (9, 53). Vero cells were infected at an m.o.i. of 1.0, and total RNA was isolated at 0, 2, 4, 6, 8, 12, 18, and 24 h.p.i. (RNeasy, Qiagen) followed by DNase I treatment (TURBO DNA-free™, Ambion). For RT-PCR analysis, one μg of total RNA was denatured at 70 °C for 5 min and reverse-transcribed using 0.4 μg of oligo(dT) primers (for mRNA RT-PCR reactions), random hexamer primers (for subsequent amplification of 18S RNA and the L gene/trailer region of the viral genome/antigenome), or negative strand-specific primers recognizing the F gene (for viral minus strand genome levels). These RT reactions included 25 nmol of dNTP and 1 μl of reverse transcriptase (RT from Stratagene) in a final volume of 20 μl. Reactions were incubated for 90 min at 48 °C. SYBR Green quantitative PCR was performed in a Roche 480 LightCycler using previously reported N, L-trailer, and negative strand F gene-specific primers and PCR cycle conditions (9, 53). Serial dilutions of p+MV were used as the RT-PCR standard for genome levels, and *in vitro* transcribed N mRNA was the standard for transcript analysis. The calculated values for the MeV transcript and genome were adjusted for variation in 18S RNA levels. The viral polymerase elongation rate was defined for primary transcription as follows: [slope of linear increase in N transcript accumulation × nucleotides in N gene transcripts]/genome level/time period in which transcript levels were monitored.

RESULTS

Box-2 Mutations affect N_{TAIL} Hydrodynamic Properties to Various Extents—We initially attempted four N amino acid substitutions, namely Gln-499, Ala-500, Ala-502, and Gly-503. Recombinant N_{TAIL}Q499E, A500D, and A502D proteins were readily expressed in *E. coli*, and their solubility was high, thus allowing recovery from the soluble fraction of the bacterial lysate. Conversely, expression and solubility of N_{TAIL} G503D was very poor. Attempts to increase both expression and solubility by modifying the temperature of induction and isopropyl β-D-thiogalactopyranoside concentration were unsuccessful and led to very low purification yields not compatible with the amounts required for the present study. Hence, production and characterization of the N_{TAIL} G503D variant was not pursued.

The N_{TAIL} Q499E, A500D, and A502D individual variants were purified to homogeneity (>95%) by immobilized metal affinity chromatography followed by gel filtration (Fig. 1*D*). The three N_{TAIL} mutated proteins migrated in SDS-PAGE with an apparent molecular mass of 20 kDa (expected molecular mass is ~14.6 kDa). This abnormal migratory behavior is well documented for parental Ed MeV N_{TAIL} (12, 18), having also been reported for all N_{TAIL} variants described thus far (21) and being due to a rather high content of acidic residues, as frequently observed in intrinsically disordered proteins (55, 56).

The Q499E and A500D N_{TAIL} variants were eluted from the gel filtration S200 column with a profile quite similar to that observed for the parental protein (see supplemental Fig. S1). Their inferred Stokes radii (~ 29 Å) are not consistent with the theoretical value (19 Å) expected for a globular conformation. Rather, the observed values are consistent with the theoretical value (28 Å) expected for a premolten globule state, as already

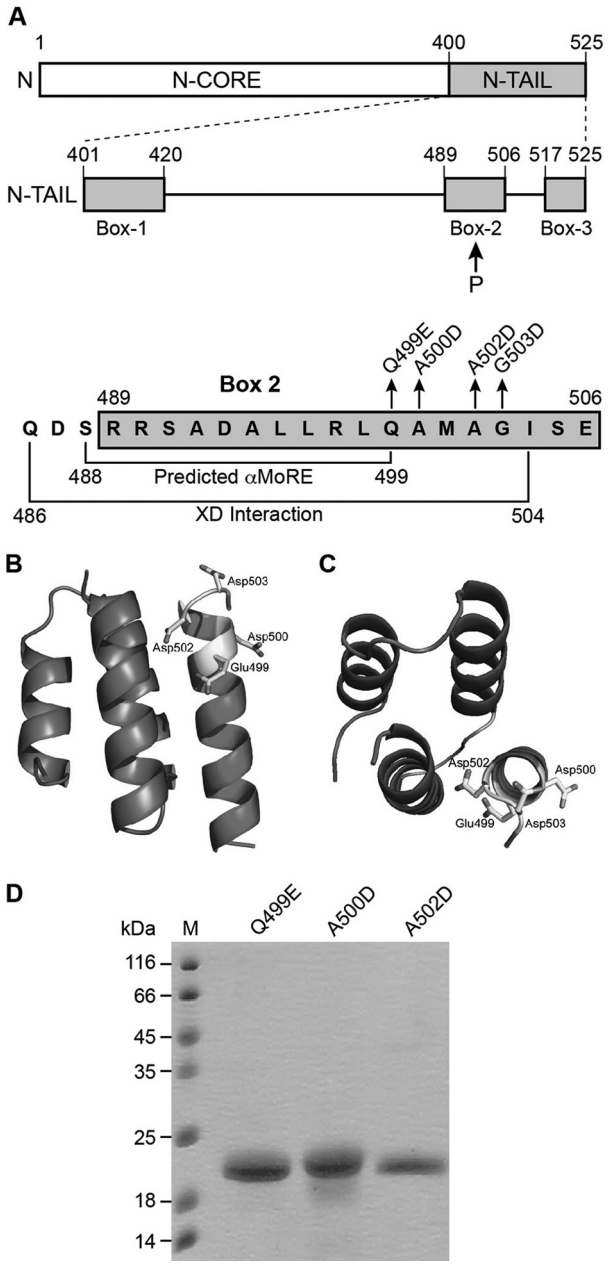

FIGURE 1. **Sequence and structural organization of the N protein C-terminal region that interacts with the P protein XD, indicating amino acid substitutions tested in the analysis of XD-N_{TAIL} structural and functional interactions.** *A*, *top*, structural organization of the N protein showing that it consists of an ordered N-terminal N_{CORE} domain and an intrinsically disordered C-terminal N_{TAIL} domain. The three N_{TAIL} regions (referred to as Box-1, -2, and -3) conserved among *Morbillivirus* members (50) are shown, where XD binds Box-2. *Bottom*, the Box-2 sequence is shown along with the amino acid substitutions generated in this study. The predicted α-MoRE and the XD-interacting sequence are shown. The region adopting an α-helical conformation in the N_{TAIL}-XD complex spans amino acids 486–502. *B* and *C*, lateral and end-on views, respectively, of the structure of XD in complex with residues 486–504 of N_{TAIL}. The side chains of the substituted amino acids (displayed as *sticks*) are shown to illustrate their relative orientation with respect to XD. Substituted amino acid side groups face away from the groove created by the three α-helices of XD for A500D (Asp-500) and G503D (Asp-503) and toward the groove for Q499E (Gln-499) and A502D (Asp-502). The structural model was obtained by replacing the side chain of the native residue in the XD/Box-2 chimera (Protein Data Bank code 1T6O) by the side chain (most frequent conformer) of the corresponding introduced amino acid. The model was then energy-minimized to avoid steric clashes by using the GROMOS96 implementation of the Swiss-PdbViewer with default parameters. *D*, Coomassie Blue staining of an 18% SDS-PAGE loaded with N_{TAIL} proteins purified from the soluble fraction of *E. coli*. *M*, molecular mass markers.

observed in the case of the parent Ed MeV N_{TAIL}. Thus, these mutated proteins share similar hydrodynamic properties with parent N_{TAIL}, being non-globular although possessing a certain residual compactness typical of the premolten globule state (39, 57–60).

Strikingly, the A502D variant displays a quite different behavior, eluting into two peaks at significantly higher elution volumes (see supplemental Fig. S1). SDS-PAGE and mass spectrometry analyses confirmed the presence of the N_{TAIL} protein in both peaks and ruled out possible degradation (data not shown). Therefore, the observed elution profile suggests that the N_{TAIL} A502D protein samples two major populations, both characterized by a much higher compactness with respect to the other N_{TAIL} proteins including the parental one. These two populations likely correspond to conformers adopting different collapsed states, with peak 2 containing the more collapsed species. Notably, the inferred Stokes radius for this latter peak is even smaller (~16 Å) than that expected for a fully folded form, implying a densely packed conformational state.

Box-2 Mutations Reduce XD-N_{TAIL} Binding Affinity Only for the A502D Variant—To estimate precisely the equilibrium dissociation constants and to ascertain possible differences in affinity for XD among the N_{TAIL} variant proteins, the N_{TAIL}-XD binding reaction was investigated by ITC, an approach that gives access to the stoichiometry, the equilibrium association constant, and the variation in enthalpy and entropy (61).

Purified native N_{TAIL} at 10 μM was loaded into the sample cell of a VP-ITC microcalorimeter and titrated with XD (from a stock solution at 150 μM), achieving a XD-N_{TAIL} molar ratio of 3 at the end of the titration (Fig. 2). The data, following integration and correction for the heats of dilution, were fitted with a standard model allowing for a set of independent and equivalent binding sites. The estimates for the model parameters (Table 1) confirmed a 1:1 stoichiometry, in agreement with previous studies (12, 17–19, 22, 24, 45), and yielded a K_D of 124 ± 6 nM, in accord with our previously published data (19). In support of the reliability of these data, similar results were obtained when N_{TAIL} was the injectant (see supplemental Fig. S2). For all of the N_{TAIL}-XD pairs studied, the binding reaction was found to be enthalpy-driven (Table 1).

In the case of the binding reaction between XD and N_{TAIL} Q499E, a K_D value (159 ± 4 nM) approximating that observed with parent N_{TAIL} was obtained following injection of increasing amounts of N_{TAIL} (Fig. 2 and Table 1), with the K_D being slightly higher (230 ± 5 nM), but within the error range observed above, when XD was used as the injectant (see supplemental Fig. S2). The N_{TAIL} A500D variant yielded a similar affinity for XD, with a K_D of 177 ± 9 nM. In all cases, the stoichiometry was close to 1 and ΔH was approximately −11 kcal/mol. In contrast, the N_{TAIL} A502D variant displayed a quite different behavior. Upon injection of XD into a 20 μM N_{TAIL} solution, saturation was not achieved even with a XD-N_{TAIL} molar ratio as high as 6, and a much lower ΔH value was obtained. In addition, the signal/noise ratio was very poor (data not shown). Subsequent experiments with N_{TAIL} A502D were therefore carried out using the ITC 200 device, which is better suited for studying binding reactions characterized by K_D val-

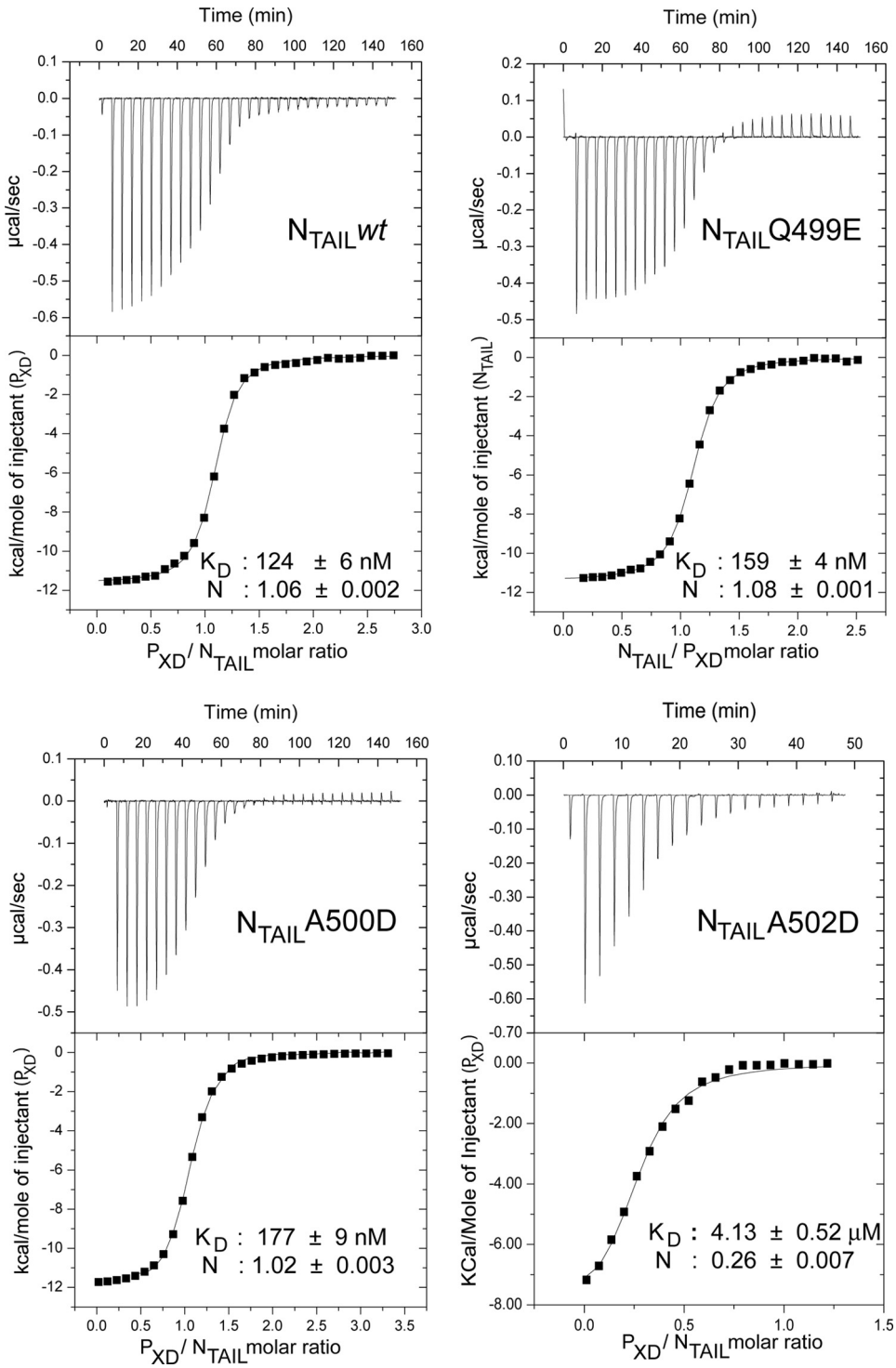

FIGURE 2. **ITC studies of binding reactions between N_{TAIL} proteins and XD.** Data are representative of at least two independent experiments. Data shown were obtained using the following initial concentrations: 12 μM N_{TAIL} and 145 μM XD for the parent N_{TAIL}-XD pair (N_{TAIL}*wt*); 14 μM XD and 155 μM N_{TAIL} for the N_{TAIL} Q499E-XD pair; 10 μM N_{TAIL} and 145 μM XD for the N_{TAIL} A500D-XD pair; and 80 μM N_{TAIL} and 500 μM XD for the N_{TAIL} A502D-XD pair. Graphs shown in the *bottom half* of each panel correspond to integrated and corrected ITC data that were fitted to a single set of site models (*i.e.* all sites identical and equivalent). In each panel, the *filled squares* represent the experimental data, and the *solid line* corresponds to the model.

ues in the μM range, being less demanding in terms of protein amounts. To confirm that the inferred values could be compared with those determined using the VP-ITC device, we repeated the experiments with parent N_{TAIL} and did indeed obtain similar binding parameters (data not shown). We then carried out binding studies in which the concentrations of both XD (used as injectant) and N_{TAIL} A502D were tuned. The following combinations of initial concentrations were assayed: 60 μM N_{TAIL}-600 μM XD, 80 μM N_{TAIL}-500 μM XD, 100 μM N_{TAIL}-500 μM XD, 100 μM N_{TAIL}-1000 μM XD, 200 μM N_{TAIL}-500 μM XD, and 200 μM N_{TAIL}-2.4 mM XD (Fig. 2 and data not shown). In all of these experiments, a stoichiometry well below

TABLE 1

Equilibrium dissociation constants and binding parameters for complex formation between XD and N_{TAIL} variants as derived from ITC studies

Data correspond to the binding curves shown in Fig. 2.

Interacting pairs	Stoichiometry	K_D	Binding enthalpy ΔH	Binding entropy ΔS
	n		*cal mol*$^{-1}$	*cal mol*$^{-1}$ *deg*$^{-1}$
N_{TAIL} *wt*-XD	1.06 ± 0.002	124 ± 6 nM	−11,610 ± 43	−8.01
N_{TAIL} Q499E-XD	1.08 ± 0.001	159 ± 4 nM	−11,400 ± 23	−7.79
N_{TAIL} A500D-XD	1.02 ± 0.003	177 ± 9 nM	−11,940 ± 80	−9.83
N_{TAIL} A502D-XD	0.26 ± 0.007	4.13 ± 0.52 μM	−8,472 ± 304	−4.26

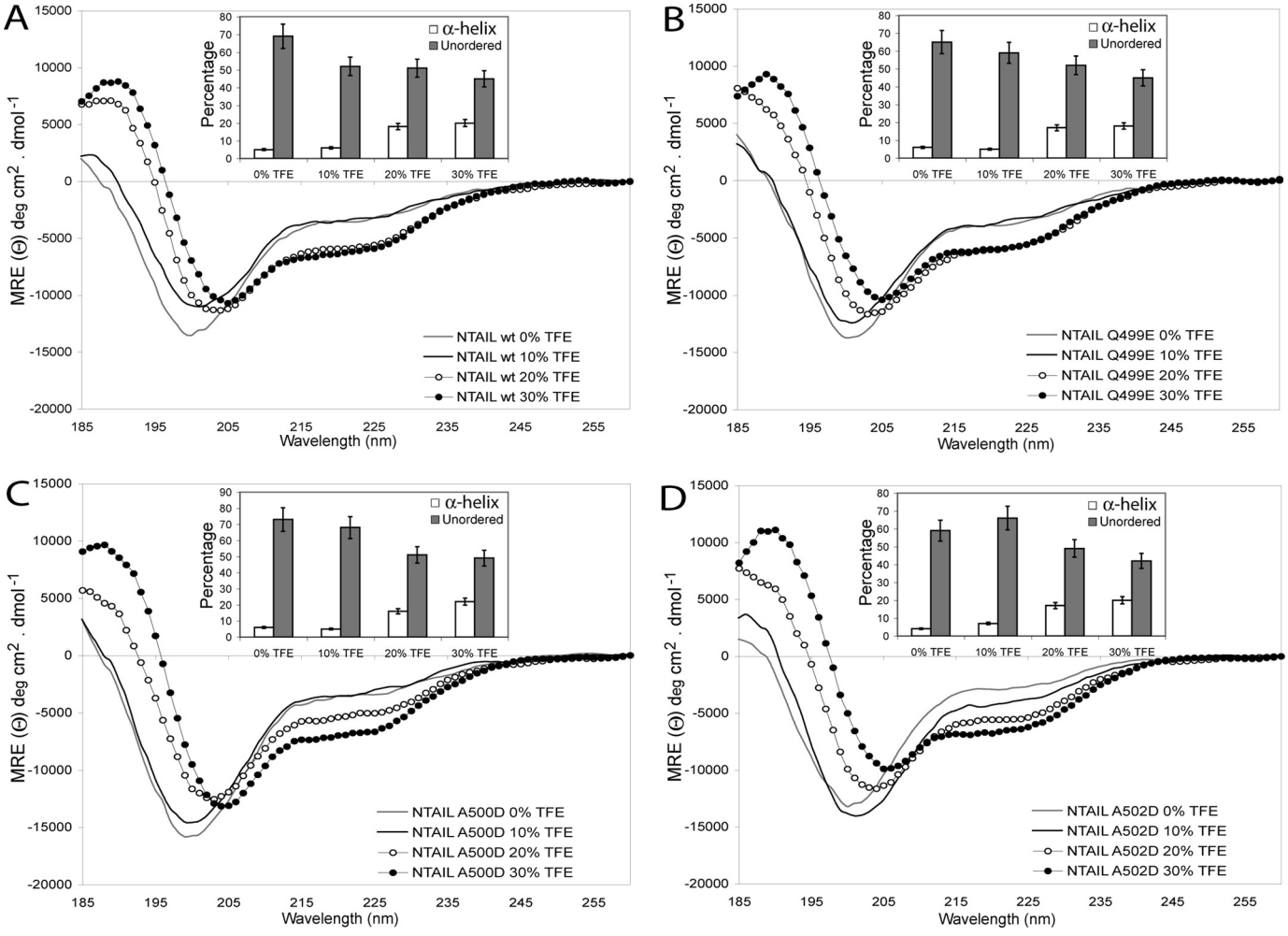

FIGURE 3. **Far-UV CD spectra and analysis of the α-helical propensities of N_{TAIL} proteins.** Shown are far-UV CD spectra of parent N_{TAIL} (*A*), N_{TAIL} Q499E (*B*), N_{TAIL} A500D (*C*), and N_{TAIL} A502D (*D*) at 0.1 mg/ml in the presence of increasing concentrations of TFE (0, 10, 20, and 30%) recorded at 20 °C. Each spectrum is the mean of three independent acquisitions. The *insets* show the α-helical and unordered content at the various TFE concentrations estimated by CDSSTR (see "Experimental Procedures"). The *error bar* (10% of the value) in each panel corresponds to the experimentally determined standard deviation from three independent experiments.

1 (and typically close to 0.25) was obtained consistently, with a K_D in the μM range (Fig. 2 and data not shown). Although the resultant binding curves typically lacked a plateau at the beginning of the titration (Fig. 2), these experiments clearly showed that the N_{TAIL} A502D variant has a much lower affinity toward XD (K_D of 4.13 ± 0.52 μM) relative to the other N_{TAIL} variants.

Box-2 Mutations Impact XD-induced Folding of N_{TAIL} to Varying Degrees—Far-UV CD was used to determine how the introduced acidic substitutions affect the overall secondary structure content of the N_{TAIL} variants. Secondary structure predictions provided by PSI-PRED (62, 63) showed no differences among the N_{TAIL} variants, with an α-helix spanning residues 488–502 being predicted as the sole secondary structure element in all cases (data not shown). To directly assess the possible impact of the acidic substitutions on the N_{TAIL} structure, the far-UV CD spectra of N_{TAIL} variants were recorded at neutral pH. The CD spectra of mutated N_{TAIL} proteins are very similar to that of parent N_{TAIL}, and all are typical of predominantly disordered proteins devoid of highly populated regular secondary structure, as seen by their large negative ellipticity at 200 nm and moderate ellipticity at 185 nm (Fig. 3). However, ellipticity values at 200 and 222 nm indicate that both mutated and parent N_{TAIL} possess some residual regular secondary structure typical of the premolten globule state. The α-helical

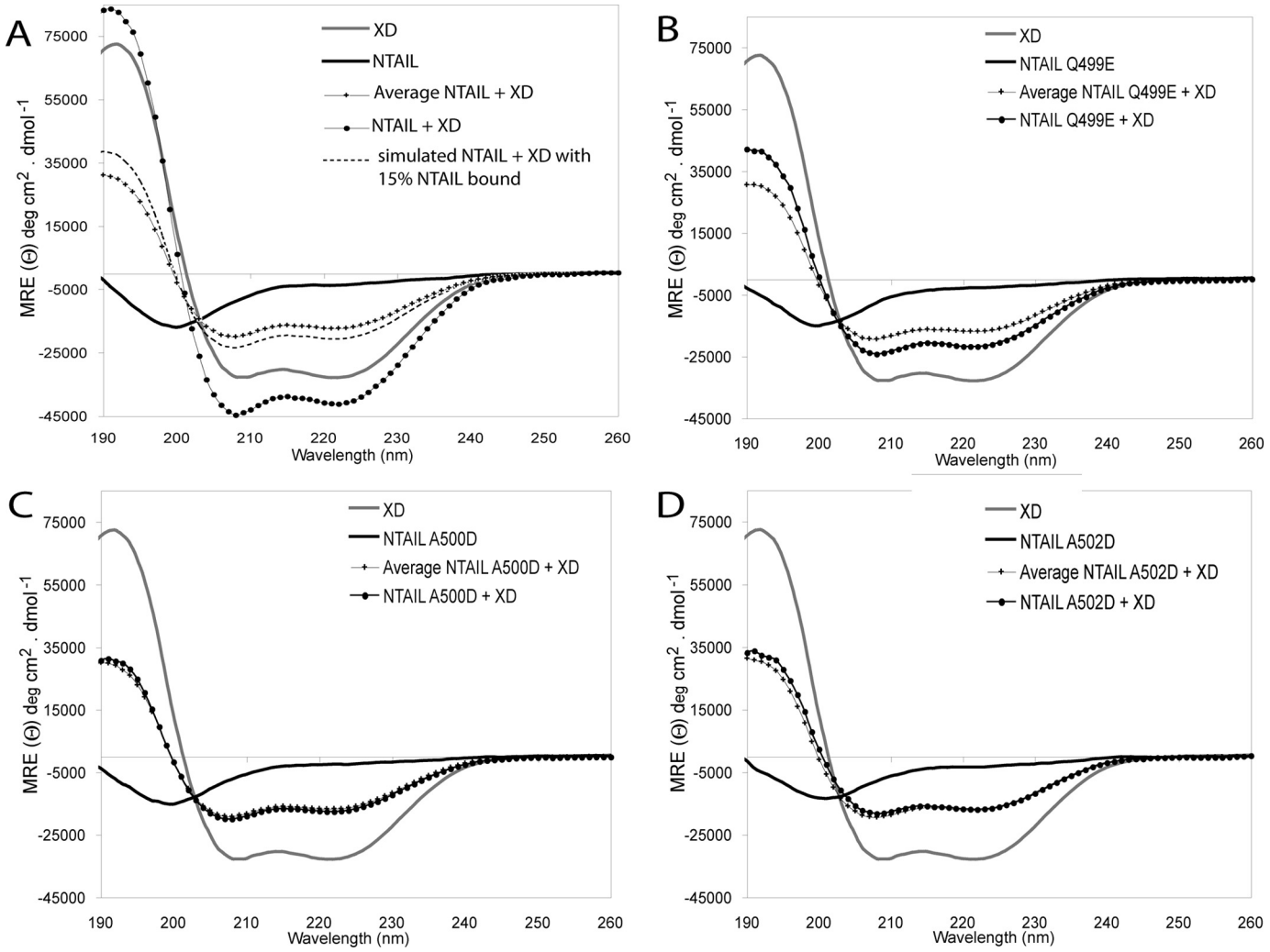

FIGURE 4. **Induced folding of N_{TAIL} proteins in the presence of XD.** Shown are far-UVCD spectra of parent N_{TAIL} (*A*), N_{TAIL} Q499E (*B*), N_{TAIL} A500D (*C*), and N_{TAIL} A502D (*D*) in the presence of a 2-fold molar excess of XD (*filled circles*). Under these conditions, the concentration of N_{TAIL} proteins and of XD is ~3.5 and 7 μM, respectively. The CD spectra of N_{TAIL} proteins alone (*black line*) or XD alone (*gray line*), as well as the theoretical average curves (*crosses*) calculated by assuming that no structural variations occur are also shown. The *dashed-line* spectrum in *A* corresponds to the simulated spectrum of a mixture containing a 2-fold molar excess of XD in which only 15% of N_{TAIL} binds to XD (see "Experimental Procedures"). Data are representative of three experimental trials.

and unordered content of the N_{TAIL} proteins, as derived by deconvolution of the spectra, showed that the N_{TAIL} variants have an α-helical content similar to parent N_{TAIL}.

To further investigate the structural impact brought about by the acidic substitutions, the structural propensities of the N_{TAIL} variants in the presence of TFE were analyzed. The solvent TFE mimics the hydrophobic environment experienced by proteins in protein-protein interactions and is therefore widely used as a probe to identify disordered regions that have a propensity to undergo induced folding (64–66). Previous studies have shown that the addition of increasing amounts of TFE to N_{TAIL} triggers a gain of α-helicity, with Box-2 playing a major role in this α-helical transition (12, 18, 19). In the present work, CD spectra of mutated N_{TAIL} proteins were recorded in the presence of increasing concentrations of TFE (Fig. 3), and the N_{TAIL} α-helical content was calculated. All proteins showed a gain of α-helicity upon addition of TFE, as indicated by the characteristic maximum at 190 nm and minima at 208 and 222 nm, thus indicating that the acidic substitutions do not impair the ability of N_{TAIL} to undergo α-helical folding. Furthermore, the mutated N_{TAIL} proteins have α-helical propensities similar to the parent N_{TAIL} protein based upon their α-helical content at different TFE concentrations. Collectively, these experiments indicate that the acidic substitutions induce little, if any, structural perturbations within N_{TAIL}.

Subsequent experiments determined whether the mutated N_{TAIL} proteins retained the ability to undergo induced folding in the presence of XD. Far-UV CD spectra were recorded in the presence of a 2-fold molar excess of XD, a condition under which XD induces the most dramatic structural transition within parent N_{TAIL} (17) (Fig. 4*A*). As a negative control, the CD spectrum of parent N_{TAIL} was recorded in the presence of lysozyme (data not shown). The far-UV CD spectrum of XD (Fig. 4, *gray line*) is typical of a structured protein with a predominant α-helical content, as indicated by the positive ellipticity between 185 and 200 nm and by the two minima at 208 and 222 nm. After mixing parent N_{TAIL} with a 2-fold molar excess of XD, the observed CD spectrum differs from the corresponding theoretical average curve calculated from the two individual spectra (Fig. 4*A*). As the theoretical average curve

corresponds to the spectrum that would be expected if no structural variations occurred, deviations from this curve indicate structural transitions. The observed deviations are consistent with an XD-induced α-helical transition of parent N_{TAIL} as judged by the much more pronounced minima at 208 and 222 nm and by the higher ellipticity at 190 nm of the experimentally observed spectrum compared with the corresponding theoretical average curve.

In the presence of a 2-fold molar excess of XD, the Q499E substitution dramatically decreases the ability of the N_{TAIL} protein to undergo α-helical folding upon binding to XD, based on the very low deviation of the experimental spectrum from the theoretical average curve (Fig. 4*B*). Under identical conditions, the A500D and the A502D substitutions fully abrogated XD-induced folding of N_{TAIL} as judged by the superimposition of the experimental and average spectra (Fig. 4, *C* and *D*). It is noteworthy that we can rule out the possibility that α-helical folding of N_{TAIL} escaped detection because of insufficient complex formation. Indeed, under the experimental conditions we used, the XD concentration is ~7 μM, a concentration well above the K_D displayed by parent, Q499E, and A500D N_{TAIL} proteins. In the case of the A502D variant, the amount of N_{TAIL} variant bound to XD would be estimated at 60% based on the total N_{TAIL} and XD concentrations used in these studies (3.6 and 7 μM, respectively) and on the K_D (4.13 μM). However, given the observed stoichiometry of 0.25 for the XD-N_{TAIL} A502D variant, the total expected amount of complex formed under these conditions is actually 15% (*i.e.* one-fourth of 60%). Lack of XD-induced folding of the A502D variant does not arise from our inability to detect folding in the subset of N_{TAIL} molecules that bind to XD. Instead, the results support a true lack of folding. This conclusion was based upon a simulated CD spectrum corresponding to a mixture containing a 2-fold molar excess of XD, where only 15% of N_{TAIL} binds (and folds) to XD. As shown in Fig. 4*A*, this simulated spectrum still deviates from the spectrum that would be obtained in the event that no structural transitions were to take place.

Box-2 N_{TAIL} Mutations Support Minireplicon Reporter Gene Expression—The impact of N_{TAIL} mutations on viral polymerase function was tested using MeV minireplicons. Subconfluent monolayers of HEp-2 cells were transfected with plasmids supporting T7 RNA polymerase-mediated expression of N, P, and L proteins and a MeV minigenome. The N plasmid directed the expression of either the parent protein or a Box-2 mutant. The minigenomic RNA contained a CAT reporter gene, with CAT activity in cell extracts reflecting the level of viral transcription and genome replication that is supported by the viral polymerase-template complex. The CAT activity in a given cell extract was normalized for differences in transfection efficiency based upon T7-mediated luciferase reporter gene expression by pT7-GL3-Luc. Transfection of HEp-2 cells was performed in triplicate for each experiment, and the resultant CAT activity was expressed as an average of 3–7 individual experiments (Fig. 5). CAT activity was not detected when transfections excluded viral polymerase (pT7MV-L) (not shown).

Box-2 mutations did not affect the expression levels of N protein based upon Western blot analysis of total protein from transfected cells (Fig. 5). All N protein variants supported viral

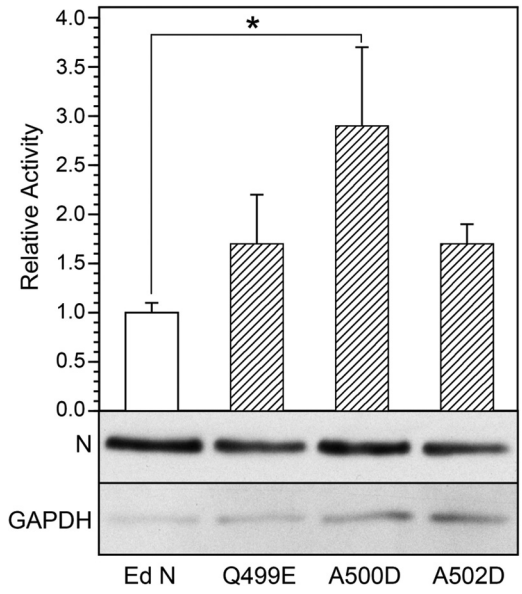

FIGURE 5. **MeV minireplicon reporter gene expression (CAT) in HEp2 cells, where the N protein template function was provided by either parent N or one of the N proteins bearing Box-2 substitutions (*i. e.* Q499E, A500D, and A502D).** Level of reporter gene expression is an average of 3–7 experimental trials, each trial representing transfections performed in triplicate. CAT activity levels were corrected for variation in transfection efficiency and expressed as a mean ± S.D. relative to the activity supported by the Ed N protein, the latter being defined as 1.0. The expression levels supported by N A502D were elevated significantly relative to Ed N ($p < 0.05$, analysis of variance). N protein levels were comparable within cells based upon Western blot analysis of total cell protein. Representative results are illustrated, with GAPDH levels used as a loading control.

polymerase activity. Statistical analysis (Bonferroni's multiple comparison test) indicated a significant (2.9-fold) increase in reporter gene expression that was supported by N A500D relative to that supported by the parent N protein ($p < 0.05$).

Both Mutant and Parent N_{TAIL} Constructs Support Comparable Polymerase Elongation Rates, although There Is Diminished Infectivity of the Mutant Viruses—Minireplicon reporter gene expression does not discriminate between transcriptase and replicase functions of the viral polymerase. We are particularly interested in the relationship between XD-N_{TAIL} interaction and transcription, given our ultimate goal of defining the mechanistic basis by which host factors enhance viral gene expression. Accordingly, recombinant infectious MeV was rescued in which the N_{TAIL} variants were encoded by the viral genome. Parent N_{TAIL} MeV was rescued in parallel. For the rescue, HEp-2 cells were transfected to express Ed N, P, and L proteins and the plus strand genomic RNA containing either the parent N gene or one of the mutated N genes encoding N (N_{TAIL}) variants.

Vero cells were infected at an m.o.i. of 0.01, and cell-free infectious viral progeny release was monitored to define multistep growth curves for each viral variant (Fig. 6). Peak progeny release occurred at 48 h.p.i. for parent N_{TAIL} MeV. MeV N Q499E and A502D exhibited similar kinetics for the elaboration of infectious viral progeny as Ed N, although there was a significant reduction in the magnitude of total and peak production, with the latter being reduced ~10-fold. In contrast, peak progeny release was comparable for parent N_{TAIL} and A500D virus, although that peak occurred at 60 h.p.i. for the mutant

virus. Maximal cytopathic effects (*i.e.* 100% syncytial coverage) correlated to the time of peak infectious progeny release.

Virus released into the supernatant of virus-infected Vero cells at 48 h.p.i. was purified by sedimentation on a discontinuous sucrose gradient, and its composition (*i.e.* genome, antigenome, defective interfering particle, viral proteins) was analyzed. The total amount of genome per unit volume was increased by 3.3-, 3.5-, and 1.6-fold for Q499E, A500D, and A502D mutants, respectively, relative to parent N_{TAIL} virus. When adjusted for infectivity titer, the results indicate reduced infectivity per unit genome by a factor of 25, 7, and 73 for Q499E, A500D, and A502D mutants, respectively. Contamination by internal deletion or copyback defective interfering particles, as determined by the ratio of genomic F segment to L-trailer segment, was only slightly increased for all mutants, with -fold changes for mutants relative to parent MeV being 1.2 for Q499E, 1.8 for A500D, and 2.3 for A502D.

Viral protein content per unit volume was greater for N_{TAIL} mutants, with a 1.6–7.8-fold increase in N and P and a 5.1–25-fold increase in M relative to parent virus. The changes followed the order A500D < A502D ≤ Q499E. Although the P/N ratios were comparable between all viruses within the range of 0.53 to 0.75, the M/N ratios in mutants were increased by a factor of 1.5–3.3 relative to the parent virus, and M/P ratios were increased by 2.3–6.2-fold (Fig. 7*B*). Notably, this magnitude of increase in viral proteins was in general agreement with the increase in genome/antigenome RNA observed in the N_{TAIL} mutants relative to parent N_{TAIL}. Consequently, as with the genome analysis, the infectivity per unit of N protein was reduced by a factor of 94 and 99 for Q499E and A502D mutants, respectively, relative to the parent N_{TAIL} virus, whereas that of the A500D mutant was comparable.

Viral production of transcript and genomic RNA was analyzed by Northern blot analysis after completion of a single virus replication cycle (24 h.p.i.) in Vero cells infected at an m.o.i. of 1.0. Increased cellular levels of both the promoter proximal N and promoter distal H transcripts and increased levels of full-length viral genomic RNA were observed for N_{TAIL} mutants relative to parent N_{TAIL} virus (Fig. 8). The differences were 1.5–1.9-fold for transcripts and 10–17-fold for genomic RNA. Kinetic analysis of viral RNA accumulation at 2, 4, 6, 8, 12, 18, and 24 h.p.i. measured by real time RT-PCR revealed that the much larger genome increases observed in Northern blots for N_{TAIL} mutants reflected in part a larger input of genomic RNA. As expected from the known delay of virus replication (9), genome levels were constant during the first ~12 h.p.i. for all viruses, after which point linear increases occurred (data not shown). The average levels of this constant input genome between 2 and 8 h.p.i. show that for a single infectious unit, genome amounts for the N_{TAIL} mutants exceed that of parent N_{TAIL} virus by factors of 26, 7, and 57 for Q499E, A500D, and A502D, respectively (Fig. 9*A*). The results of quantification using L-trailer primers or primers specific to the minus strand F genome paralleled one another for all times points examined, thus excluding a major contamination of the virus stocks by subgenomic defective interfering particles and a significant excess of defective interfering particles production during virus infection (not shown). The 57-fold difference between A502D and parent N_{TAIL} virus was statistically significant ($p < 0.05$, analysis of variance). This higher level of input genome for

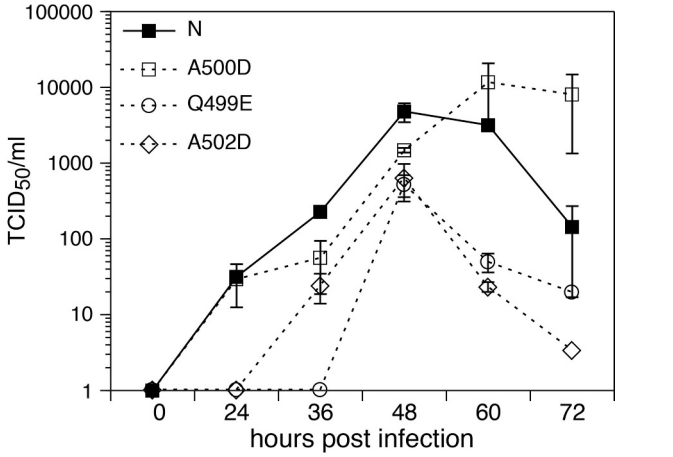

FIGURE 6. **Multistep growth curves of the infectious MeV Box-2 mutants in Vero cells infected at an m.o.i. of 0.01.** Culture supernatant was collected at 12-h intervals for the titration of cell-free infectious viral progeny reported as the 50% tissue culture infective dose ($TCID_{50}$). Infections were performed in triplicate with results expressed as a mean ± S.D.

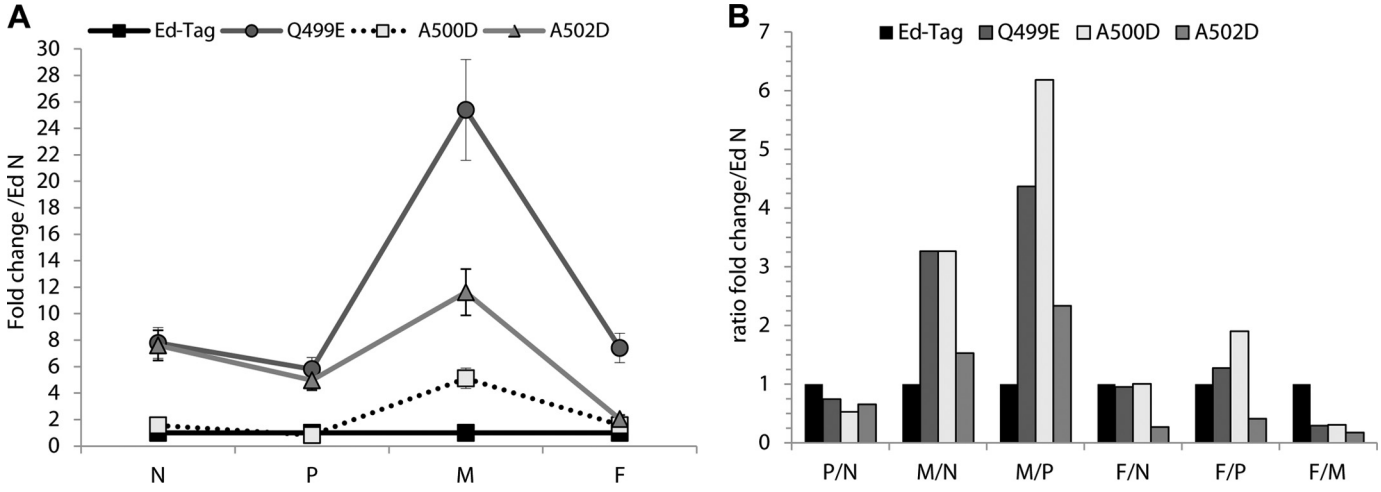

FIGURE 7. **Viral protein contents of purified virions from N_{TAIL} mutants (*A*) and protein ratios (*B*) normalized to parental Ed N virus.** MeV N, P, M, and F proteins were quantified after adsorption of serially diluted purified virus on nitrocellulose and immunolabeling with antigen-specific monoclonal antibodies.

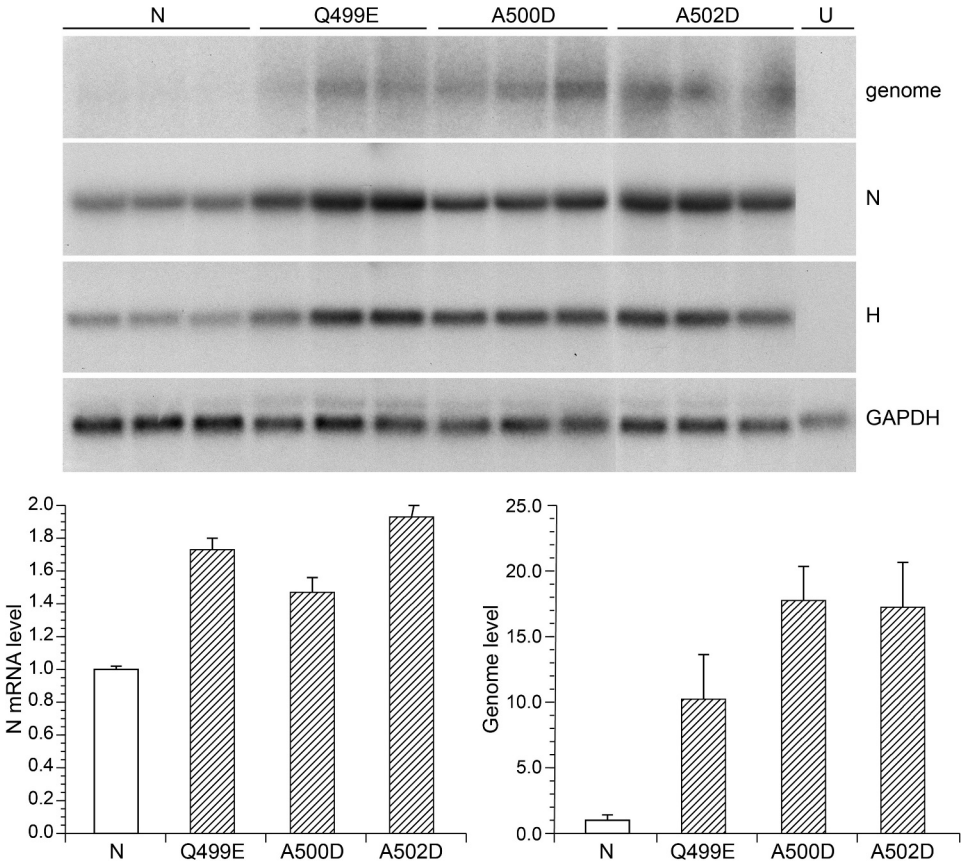

FIGURE 8. **Northern blot analysis of MeV transcript and genome levels in Vero cells infected with Ed N, A500D, Q499E or A502D.** Infections were performed in triplicate at an m.o.i. of 1, and RNA was harvested at 24 h.p.i. *U*, represents RNA from uninfected control cells. The 15-kb genome was detected with a negative strand-specific ^{32}P-labeled riboprobe corresponding to the F gene, and N and H transcripts were detected with plus strand-specific riboprobes. GAPDH-corrected signal intensities were expressed relative to levels produced by Ed N MeV. Increases in transcript and genome levels for the mutants relative to parent virus were statistically significant.

mutant viruses is consistent with their reduced infectivity relative to the parent virus, given that the m.o.i. was constant. Transcript analysis focused on the N gene. Increases in transcript levels were linear between 0 and 6 h.p.i., with R^2 values of 0.98–0.99 (Fig. 9*B*). This defines the period of primary transcription (*i.e.* transcription of incoming genomic templates by preformed transcriptases) in which an apparent polymerase elongation rate can be calculated. During this phase, slopes describing the linear increase in transcript levels are used as a measure of polymerase (transcriptase) activity, corrected for variation in genome levels (9, 53). The calculation assumes that every incoming genome is transcriptionally active and that the number of active transcriptases is similar for every mutant. The calculated rate of parent N_{TAIL} virus polymerase was 2.3 nucleotides/s, which closely approximates the 3.0 nucleotides/s reported for this virus and Hallé MeV strain on HeLa and 293T cells (9). Rates for the Box-2 mutant viruses were within a 1.7-fold range of that measured for parent N_{TAIL} virus (Fig. 9*C*).

DISCUSSION

In this study, we created amino acid substitutions at three positions within the Box-2 region of N_{TAIL} (*e.g.* the primary XD-binding site) with the specific purpose of assessing the possible relationships among N_{TAIL}-XD binding affinity, XD-induced α-helical folding of N_{TAIL}, and polymerase activity. Contrary to our hypothesis, XD-induced folding was not required to maintain a high XD-N_{TAIL} binding affinity, and loss of XD-induced N_{TAIL}-α-helical folding or binding affinity had no significant effect on polymerase activity. Rather unexpectedly, however, these substitutions were found to affect virus infectivity strongly, thus arguing for a possible role for Box-2 in assuring the fidelity of polymerase activity or particle assembly.

Indeed, according to our results, MeV polymerase activity is maintained within a relatively narrow range when XD-induced α-helical folding of N_{TAIL} is reduced or eliminated, even when XD-N_{TAIL} affinity is reduced by over 30-fold. The ITC experiments confirmed the 1:1 stoichiometry of the N_{TAIL}-XD binding reaction and yielded a K_D of 124 ± 6 nM, in accord with our previously published data (12, 17–19, 22, 24, 45). A recent study by Kingston and colleague (67) characterized the binding reactions between XD and synthetic peptides corresponding to amino acids 477–505 or 477–525 of N, deriving a K_D that was either 7.4 or 15 μM, respectively. The discrepancy between our data and those of Kingston (67) likely reflects the use of full-length N_{TAIL} *versus* N_{TAIL} peptides, respectively. A K_D for XD/full-length N_{TAIL} binding reactions in the 100 nM range was obtained using surface plasmon resonance analysis, fluorescence spectroscopy, and ITC, supporting the view that it is the protein reactants, and not the analytical approach, that are

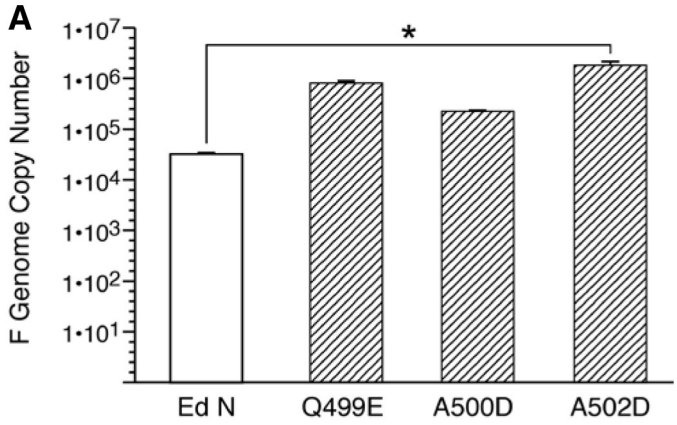

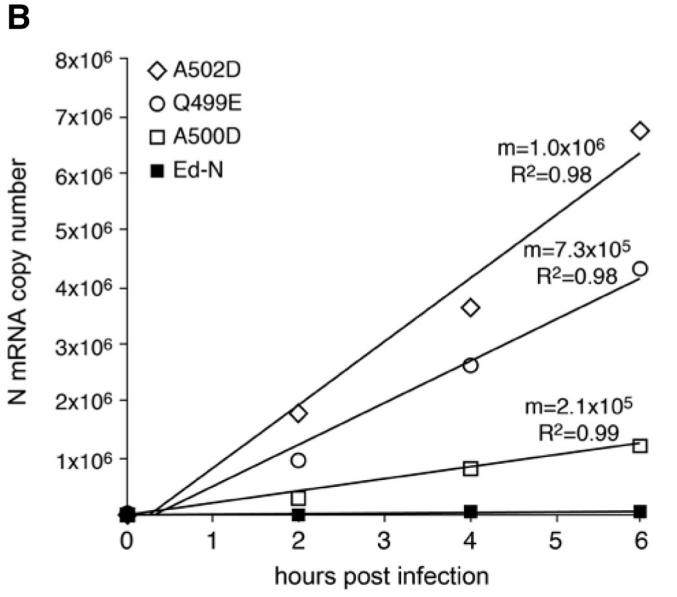

C

Calculated transcript elongation rates:

Ed N	2.3 nt/s
NQ499E	3.9 nt/s
NA500D	4.1 nt/s
NA502D	1.3 nt/s

FIGURE 9. **Real time RT-PCR analysis of viral genome and transcript levels in Vero cells infected with Ed N, A500D, Q499E or A502D.** Infections were performed in triplicate at an m.o.i. of 1, and RNA was harvested at 0–8 h.p.i.; the results were used to calculate the transcriptase elongation rate. *A*, input genome levels reflecting the mean ± S.D. for all time points. Results are representative of two experimental trials. *B*, linear regression analysis of viral N transcript levels used oligo(dT)-primed cDNAs. Each infection was performed in duplicate, and the N mRNA copy number is expressed as a mean. Reactions lacking RT and analysis of uninfected samples were included as negative controls (not shown). Experimental data over time showed a good linear fit (R^2 values > 0.95), consistent with viral primary transcription accumulation. *m*, represents the number of N mRNA copies produced per h. Results are representative of two experimental trials. *C*, calculated transcriptase elongation rate based upon the slope of transcript accumulation and corrected for variance in genome levels.

the basis for the discrepancy. N_{TAIL} Q499E and A500D exhibited a binding affinity for XD that was comparable to parent N_{TAIL}, whereas the XD affinity of N_{TAIL} A502D was significantly reduced. The latter may reflect conformational differences between A502D and the other constructs, with these differences being supported by size exclusion chromatography studies that point out a unique conformational behavior for N_{TAIL} A502D. Indeed, this latter variant was found to populate two distinct conformational states, both characterized by a high degree of compactness. The higher extent of compactness of N_{TAIL} A502D likely arises from the establishment of tertiary contacts (whether short or long range) and does not reflect an increased content in regular secondary structure, in accord with our recent results indicating that the content in regular secondary structure is not a major determinant of protein compaction (68). In agreement with this hypothesis, although both mutated and parent N_{TAIL} possess some residual regular secondary structure typical of the premolten globule state, CD studies did show that N_{TAIL} A502D possesses an α-helical content that is even slightly lower than that of the other N_{TAIL} proteins. This raises the possibility of a less stably configured prerecognition state as a possible basis for the reduced affinity of XD for N_{TAIL} A502D. On the other hand, it is also conceivable that the more collapsed state adopted by N_{TAIL} A502D could lead to the sequestering of the XD-binding site, thereby rendering this variant less competent to binding. That MoREs can escape binding to partners through functional misfolding of the intrinsically disordered protein has already been reported (69).

The stoichiometry below 1 that was observed for the N_{TAIL} A502D-XD binding reaction likely reflects the reduced capacity of this N_{TAIL} variant to bind to XD. A stoichiometry below 1 can reflect errors in the estimates of protein concentrations or the inability of a significant proportion of titrate to interact with the titrant. Because the same XD sample was used in all ITC studies, possible errors in the estimates of XD concentration that might have specifically confounded the analyses of N_{TAIL} A502D could be ruled out. Likewise, errors in the estimate of the N_{TAIL} A502D concentration could be excluded as judged by SDS-PAGE of N_{TAIL} variants. That this reduced capacity does not arise from the aggregation of N_{TAIL} A502D or XD has been ruled out by dynamic light scattering studies that detected no aggregates even at concentrations as high as 170 μM (N_{TAIL} A502D) and 2.4 mM (XD) (data not shown). It is thus conceivable that a stoichiometry of 0.25 could reflect a conformational heterogeneity of N_{TAIL} A502D, where 75% of the N_{TAIL} conformers would not be competent to bind XD. It is tempting to speculate that the N_{TAIL} conformers unable to bind to XD could correspond to a highly compact form (such as that actually observed in size exclusion chromatography studies) in which the XD-binding site would be sequestered within the protein and hence inaccessible for binding.

Although CD studies under conditions mimicking the hydrophobic environment of protein-protein interactions (*i.e.* in the presence of TFE) failed to unveil significant differences in the folding abilities of N_{TAIL} proteins, studies carried out in the presence of the binding partner revealed that the acidic substitutions did impact the ability of N_{TAIL} to undergo XD-induced

folding. The Q499E substitution significantly reduced the ability of N_{TAIL} to undergo α-helical folding in the presence of XD, and the A500D and A502D substitutions fully abrogated it. A plausible explanation for the observed discrepancy between studies making use of TFE *versus* XD may reside in the global nature of the structural effects triggered by TFE (where TFE may promote folding of N_{TAIL} sites other than Box-2, such as Box-1 (20)) and in the fact that TFE is a much less sensitive probe of local structural transitions than the true partner. This latter point is well illustrated by previous EPR studies showing that XD triggers a much more pronounced reduction in the mobility of spin labels grafted within Box-2 as compared with TFE (21).

It is noteworthy that the failure of XD to induce significant N_{TAIL} A502D folding does not likely reflect the elevated K_D (relative to parent Ed N_{TAIL}) given the molar excess of XD that was used in these experiments and the fact that a simulated CD demonstrated the ability to detect induced folding when only a subset of N_{TAIL} binds XD. Likewise, the possibility that XD-induced α-helical folding of N_{TAIL} occurs but escapes detection due to possible differences between the time scale with which structural transitions take place and the time window of detection can be ruled out, given the low (below femtoseconds) time scale of CD and the typical nanosecond to microsecond time scale of structural transitions. As a consequence of this latter property, any CD spectrum can be resolved into the component spectra of the main conformer types (α-helix, β-sheet, turns, and random coils).

Importantly, our results showed that XD-induced α-helical folding of N_{TAIL} is not a basis for the relatively high affinity of the XD-N_{TAIL} complex (*i.e.* induced α-helical folding of N_{TAIL} is not strictly required to stabilize the complex). XD-induced α-helical folding was significantly reduced for N_{TAIL} Q499E and completely abrogated for A500D based upon the CD analyses, despite the fact that XD-N_{TAIL} binding affinity was maintained at a level comparable to that of parent N_{TAIL}. The finding that α-helical folding is not strictly required for the formation of a stable complex implies that XD would be able to bind to N_{TAIL} conformers that lack a transiently populated α-helix, supporting previous spectroscopic data arguing for a mixed mechanism of N_{TAIL}-XD complex formation relying on both conformational selection and folding after binding (24).

Minireplicon reporter gene expression and estimates of viral transcript elongation rates for A502D, where XD-N_{TAIL} binding affinity was reduced by more than 30-fold relative to parent virus, also argues against the idea that the relatively high XD-N_{TAIL} binding affinity imposes constraint on (*i.e.* slows down) viral transcriptase function. Minireplicon reporter gene expression was not significantly increased for A502D relative to the other viruses. In addition, the calculated transcriptase elongation rate was actually slightly reduced (*i.e.* the rate was reduced by 43% relative to parent virus), although the latter finding may in part reflect the fact that not all cytoplasmic nucleocapsids contributes equally to transcription. That P/N_{TAIL} binding affinity is not the primary determinant of the relatively slow polymerase elongation rate of MeV is supported by observations in a related paramyxovirus: the polymerase elongation rate of Sendai virus is 1.7 nt/s, whereas the P/N complex has a K_D of 60 μM (70).

Despite the diminished capacity of isolated N_{TAIL} A502D to bind XD, there was no apparent change in the P to N ratio in the composition of cell-free virions. Here, the oligomeric state of P interacting with the 2649 N monomers of an intact nucleocapsid may combine to assure that there are ample N_{TAIL} conformers capable of engaging polymerase complexes to levels observed in parent virus. Likewise, globally the comparison of polymerase functions as transcriptase and replicase determined both in a minigenome assay and in the context of viable recombinant virus indicates a lack of major impact of either less pronounced induced folding of N_{TAIL} or a >30-fold reduction in N_{TAIL} affinity to XD.

In contrast, the induced folding of N_{TAIL} and maintenance of a relatively high N_{TAIL}-XD binding affinity appears to be essential for maintaining optimal infectivity of MeV. This observation is consistent with the high degree to which amino acids targeted in the current work are conserved among measles isolates. Indeed, based on the analysis of more than 4000 MeV N protein sequences available in the databases, Box-2 is very poorly variable, and the lack of natural variants exhibiting the substitutions we have introduced argues for the amino acid sequence of Box-2 as being under a highly selective pressure. Consequently, one could predict that upon repeated passages *in vitro* and/or *in vivo* of the N mutants we have designed, a reversion to the parental sequence should be observed.

The drop in infectivity of N_{TAIL} mutants could not be attributed to significant changes in RNA synthesis and *N*-encapsidation of genome, to increased defective interfering particle production, or to overt changes in the protein composition of the virus particles. Likewise, because dot blot analysis of the viral protein composition was performed by diluting intact virus particles (and not solubilized viruses), we can also exclude a major change in the size and polyploidy (71, 72) of the virions based upon the relatively unchanged genome/N protein ratio.

The basis for reduced infectivity of the N_{TAIL} mutants is currently unknown. Sequences C-terminal to N_{TAIL} Box-2 may interact with other viral and/or cellular factors required to assure the efficient use of every nucleocapsid template and the fidelity of transcription and/or genome replication, where optimal interaction depends upon specific and highly conserved N_{TAIL} conformers. Measles virus matrix protein interacts with the nucleocapsid (73–75) and promotes virus assembly and particle release (76). In addition, M negatively regulates virus transcription by binding to the C terminus N_{TAIL} dileucine 523–524 motif (77, 78). Moreover, in virus particles and infected cells, many nucleocapsids are partially covered by the M protein (79 – 81), where discontinuous helices of M mediate nucleocapsid folding (72). Thus, for nucleocapsid delivered into the cytoplasm after virus entry, the incoming transcriptase will have to displace M polymers as it progresses downstream along the encapsidated genome. Likewise, later in the virus infection cycle, as M gene expression increases, the replicase will have to compete with the ongoing M polymerization. Because of the apparent heterogeneity of nucleocapsid coverage by the M protein (72), we can speculate that alteration of Box2-XD interactions can influence M and P competition for N_{TAIL} binding.

Enhanced M binding, supported by the 1.5–3.3-fold increase in M/N ratios in virions, could increase the chance of producing nucleocapsids unsuitable for supporting an entire virus replication cycle. Further work is needed to support this hypothesis. As for the fidelity of polymerase function, it is possible that the error rate of the polymerase is increased, leading to subtle changes in the genome sequence that disrupt infectivity. This possibility will require full genome sequencing to illuminate.

Collectively, this work provides a new perspective for the study of viral polymerase activity and its modulation by viral and host factors. The currently accepted model whereby the N_{TAIL}-XD interaction has to be relatively weak to allow the polymerase to cartwheel on the nucleocapsid template needs to be revisited in light of the present results. The N_{TAIL} region C-terminal to Box-2 comprises a regulatory domain that can impose constraint on polymerase activity (47). Our results suggest that this regulatory domain acts not by directly influencing cycles of binding and release by the polymerase complex but rather by mediating the interaction with other factors that may positively or negatively influence polymerase function. Further development of our understanding of the relationship between XD-induced N_{TAIL} folding and the fidelity and level of viral polymerase activity will require knowledge of the composition of the viral RNA-dependent RNA polymerase in transcriptase *versus* replicase mode. Indeed, the replicase and transcriptase of vesicular stomatitis virus, another Mononegavirales, have been shown to differ in both viral and cellular protein components (28).

Acknowledgments—We thank Elodie Liquière and Jean-Marie Bourhis for technical help in generating the bacterial expression plasmids encoding mutated N_{TAIL} proteins. We also thank Louis-Marie Bloyet for mathematical analysis of the dot blot data.

REFERENCES

1. Ruigrok, R. W., Crépin, T., and Kolakofsky, D. (2011) Nucleoproteins and nucleocapsids of negative-strand RNA viruses. *Curr. Opin. Microbiol.* **14,** 504–510
2. Gerlier, D., and Lyles, D. S. (2011) Interplay between innate immunity and negative-strand RNA viruses: towards a rational model. *Microbiol. Mol. Biol. Rev.* **75,** 468–490
3. Mühlebach, M. D., Mateo, M., Sinn, P. L., Prüfer, S., Uhlig, K. M., Leonard, V. H., Navaratnarajah, C. K., Frenzke, M., Wong, X. X., Sawatsky, B., Ramachandran, S., McCray, P. B., Jr., Cichutek, K., von Messling, V., Lopez, M., and Cattaneo, R. (2011) Adherens junction protein nectin-4 is the epithelial receptor for measles virus. *Nature* **480,** 530–533
4. Plemper, R. K., Brindley, M. A., and Iorio, R. M. (2011) Structural and mechanistic studies of measles virus illuminate paramyxovirus entry. *PLoS Pathog.* **7,** e1002058
5. Yanagi, Y., Takeda, M., Ohno, S., and Hashiguchi, T. (2009) Measles virus receptors. *Curr. Top. Microbiol. Immunol.* **329,** 13–30
6. Gerlier, D., and Valentin, H. (2009) Measles virus interaction with host cells and impact on innate immunity. *Curr. Top. Microbiol. Immunol.* **329,** 163–191
7. Desfosses, A., Goret, G., Farias Estrozi, L., Ruigrok, R. W., and Gutsche, I. (2011) Nucleoprotein-RNA orientation in the measles virus nucleocapsid by three-dimensional electron microscopy. *J. Virol.* **85,** 1391–1395
8. Tawar, R. G., Duquerroy, S., Vonrhein, C., Varela, P. F., Damier-Piolle, L., Castagné, N., MacLellan, K., Bedouelle, H., Bricogne, G., Bhella, D., Eléouët, J. F., and Rey, F. A. (2009) Crystal structure of a nucleocapsid-like nucleoprotein-RNA complex of respiratory syncytial virus. *Science* **326,** 1279–1283
9. Plumet, S., Duprex, W. P., and Gerlier, D. (2005) Dynamics of viral RNA synthesis during measles virus infection. *J. Virol.* **79,** 6900–6908
10. Lamb, R. A., and Kolakofsky, D. (2001) Paramyxoviridae: the viruses and their replication. In *Fields Virology* (Fields, B. N., Knipe, D. M., and Howley, P. M., eds) 4th Ed., pp. 1305–1340, Lippincott-Raven, Philadelphia, PA
11. Longhi, S. (2009) Nucleocapsid structure and function. *Curr. Top. Microbiol. Immunol.* **329,** 103–128
12. Longhi, S., Receveur-Bréchot, V., Karlin, D., Johansson, K., Darbon, H., Bhella, D., Yeo, R., Finet, S., and Canard, B. (2003) The C-terminal domain of the measles virus nucleoprotein is intrinsically disordered and folds upon binding to the C-terminal moiety of the phosphoprotein. *J. Biol. Chem.* **278,** 18638–18648
13. Tarbouriech, N., Curran, J., Ebel, C., Ruigrok, R. W., and Burmeister, W. P. (2000) On the domain structure and the polymerization state of the sendai virus P protein. *Virology* **266,** 99–109
14. Tarbouriech, N., Curran, J., Ruigrok, R. W., and Burmeister, W. P. (2000) Tetrameric coiled coil domain of Sendai virus phosphoprotein. *Nat. Struct. Biol.* **7,** 777–781
15. Ding, H., Green, T. J., Lu, S., and Luo, M. (2006) Crystal structure of the oligomerization domain of the phosphoprotein of vesicular stomatitis virus. *J. Virol.* **80,** 2808–2814
16. Ivanov, I., Crépin, T., Jamin, M., and Ruigrok, R. W. (2010) Structure of the dimerization domain of the rabies virus phosphoprotein. *J. Virol.* **84,** 3707–3710
17. Johansson, K., Bourhis, J. M., Campanacci, V., Cambillau, C., Canard, B., and Longhi, S. (2003) Crystal structure of the measles virus phosphoprotein domain responsible for the induced folding of the C-terminal domain of the nucleoprotein. *J. Biol. Chem.* **278,** 44567–44573
18. Bourhis, J. M., Johansson, K., Receveur-Bréchot, V., Oldfield, C. J., Dunker, K. A., Canard, B., and Longhi, S. (2004) The C-terminal domain of measles virus nucleoprotein belongs to the class of intrinsically disordered proteins that fold upon binding to their physiological partner. *Virus Res.* **99,** 157–167
19. Bourhis, J. M., Receveur-Bréchot, V., Oglesbee, M., Zhang, X., Buccellato, M., Darbon, H., Canard, B., Finet, S., and Longhi, S. (2005) The intrinsically disordered C-terminal domain of the measles virus nucleoprotein interacts with the C-terminal domain of the phosphoprotein via two distinct sites and remains predominantly unfolded. *Protein Sci.* **14,** 1975–1992
20. Morin, B., Bourhis, J. M., Belle, V., Woudstra, M., Carrière, F., Guigliarelli, B., Fournel, A., and Longhi, S. (2006) Assessing induced folding of an intrinsically disordered protein by site-directed spin-labeling electron paramagnetic resonance spectroscopy. *J. Phys. Chem. B* **110,** 20596–20608
21. Belle, V., Rouger, S., Costanzo, S., Liquière, E., Strancar, J., Guigliarelli, B., Fournel, A., and Longhi, S. (2008) Mapping α-helical induced folding within the intrinsically disordered C-terminal domain of the measles virus nucleoprotein by site-directed spin-labeling EPR spectroscopy. *Proteins* **73,** 973–988
22. Bernard, C., Gely, S., Bourhis, J. M., Morelli, X., Longhi, S., and Darbon, H. (2009) Interaction between the C-terminal domains of N and P proteins of measles virus investigated by NMR. *FEBS Lett.* **583,** 1084–1089
23. Bischak, C. G., Longhi, S., Snead, D. M., Costanzo, S., Terrer, E., and Londergan, C. H. (2010) Probing structural transitions in the intrinsically disordered C-terminal domain of the measles virus nucleoprotein by vibrational spectroscopy of cyanylated cysteines. *Biophys. J.* **99,** 1676–1683
24. Gely, S., Lowry, D. F., Bernard, C., Jensen, M. R., Blackledge, M., Costanzo, S., Bourhis, J. M., Darbon, H., Daughdrill, G., and Longhi, S. (2010) Solution structure of the C-terminal X domain of the measles virus phosphoprotein and interaction with the intrinsically disordered C-terminal domain of the nucleoprotein. *J. Mol. Recognit.* **23,** 435–447
25. Kavalenka, A., Urbancic, I., Belle, V., Rouger, S., Costanzo, S., Kure, S., Fournel, A., Longhi, S., Guigliarelli, B., and Strancar, J. (2010) Conformational analysis of the partially disordered measles virus N(TAIL)-XD complex by SDSL EPR spectroscopy. *Biophys. J.* **98,** 1055–1064
26. Jensen, M. R., Communie, G., Ribeiro, E. A., Jr., Martinez, N., Desfosses, A., Salmon, L., Mollica, L., Gabel, F., Jamin, M., Longhi, S., Ruigrok, R. W.,

and Blackledge, M. (2011) Intrinsic disorder in measles virus nucleocapsids. *Proc. Natl. Acad. Sci. U.S.A.* **108,** 9839–9844
27. Longhi, S. (2011) Structural disorder within the measles virus nucleoprotein and phosphoprotein: functional implications for transcription and replication. In *Negative Strand RNA Virus* (Luo, M., ed) pp. 95–125, World Scientific Publishing, Singapore
28. Qanungo, K. R., Shaji, D., Mathur, M., and Banerjee, A. K. (2004) Two RNA polymerase complexes from vesicular stomatitis virus-infected cells that carry out transcription and replication of genome RNA. *Proc. Natl. Acad. Sci. U.S.A.* **101,** 5952–5957
29. Karlin, D., Ferron, F., Canard, B., and Longhi, S. (2003) Structural disorder and modular organization in Paramyxovirinae N and P. *J. Gen. Virol.* **84,** 3239–3252
30. Habchi, J., Mamelli, L., Darbon, H., and Longhi, S. (2010) Structural disorder within *Henipavirus* nucleoprotein and phosphoprotein: from predictions to experimental assessment. *PLoS ONE* **5,** e11684
31. Habchi, J., and Longhi, S. (2012) Structural disorder within paramyxovirus nucleoproteins and phosphoproteins. *Mol. Biosyst.* **8,** 69–81
32. Habchi, J., Mamelli, L., and Longhi, S. (2012) Structural disorder within the nucleoprotein and phosphoprotein from measles, Nipah and Hendra viruses. In *Flexible Viruses: Structural Disorder in Viral Proteins* (Uversky, V. N., and Longhi, S., eds) pp. 47–94, John Wiley and Sons, Hoboken, NJ
33. Wright, P. E., and Dyson, H. J. (1999) Intrinsically unstructured proteins: re-assessing the protein structure-function paradigm. *J. Mol. Biol.* **293,** 321–331
34. Dunker, A. K., Oldfield, C. J., Meng, J., Romero, P., Yang, J. Y., Chen, J. W., Vacic, V., Obradovic, Z., and Uversky, V. N. (2008) The unfoldomics decade: an update on intrinsically disordered proteins. *BMC Genomics* **9,** Suppl. 2, S1
35. Dunker, A. K., Silman, I., Uversky, V. N., and Sussman, J. L. (2008) Function and structure of inherently disordered proteins. *Curr. Opin. Struct. Biol.* **18,** 756–764
36. Uversky, V. N. (2010) The mysterious unfoldome: structureless, underappreciated, yet vital part of any given proteome. *J. Biomed. Biotechnol.* **2010,** 568068
37. Uversky, V. N., and Dunker, A. K. (2010) Understanding protein nonfolding. *Biochim. Biophys. Acta* **1804,** 1231–1264
38. Turoverov, K. K., Kuznetsova, I. M., and Uversky, V. N. (2010) The protein kingdom extended: ordered and intrinsically disordered proteins, their folding, supramolecular complex formation, and aggregation. *Prog. Biophys. Mol. Biol.* **102,** 73–84
39. Dunker, A. K., Lawson, J. D., Brown, C. J., Williams, R. M., Romero, P., Oh, J. S., Oldfield, C. J., Campen, A. M., Ratliff, C. M., Hipps, K. W., Ausio, J., Nissen, M. S., Reeves, R., Kang, C., Kissinger, C. R., Bailey, R. W., Griswold, M. D., Chiu, W., Garner, E. C., and Obradovic, Z. (2001) Intrinsically disordered protein. *J. Mol. Graph. Model.* **19,** 26–59
40. Linding, R., Jensen, L. J., Diella, F., Bork, P., Gibson, T. J., and Russell, R. B. (2003) Protein disorder prediction: implications for structural proteomics. *Structure* **11,** 1453–1459
41. Oldfield, C. J., Cheng, Y., Cortese, M. S., Romero, P., Uversky, V. N., and Dunker, A. K. (2005) Coupled folding and binding with α-helix-forming molecular recognition elements. *Biochemistry* **44,** 12454–12470
42. Mohan, A., Oldfield, C. J., Radivojac, P., Vacic, V., Cortese, M. S., Dunker, A. K., and Uversky, V. N. (2006) Analysis of molecular recognition features (MoRFs). *J. Mol. Biol.* **362,** 1043–1059
43. Vacic, V., Oldfield, C. J., Mohan, A., Radivojac, P., Cortese, M. S., Uversky, V. N., and Dunker, A. K. (2007) Characterization of molecular recognition features, MoRFs, and their binding partners. *J. Proteome Res.* **6,** 2351–2366
44. Fuxreiter, M., Tompa, P., and Simon, I. (2007) Local structural disorder imparts plasticity on linear motifs. *Bioinformatics* **23,** 950–956
45. Kingston, R. L., Hamel, D. J., Gay, L. S., Dahlquist, F. W., and Matthews, B. W. (2004) Structural basis for the attachment of a paramyxoviral polymerase to its template. *Proc. Natl. Acad. Sci. U.S.A.* **101,** 8301–8306
46. Longhi, S., and Oglesbee, M. (2010) Structural disorder within the measles virus nucleoprotein and phosphoprotein. *Protein Pept. Lett.* **17,** 961–978
47. Zhang, X., Glendening, C., Linke, H., Parks, C. L., Brooks, C., Udem, S. A., and Oglesbee, M. (2002) Identification and characterization of a regulatory domain on the carboxyl terminus of the measles virus nucleocapsid protein. *J. Virol.* **76,** 8737–8746
48. Whitmore, L., and Wallace, B. A. (2004) DICHROWEB, an online server for protein secondary structure analyses from circular dichroism spectroscopic data. *Nucleic Acids Res.* **32,** W668–673
49. Whitmore, L., and Wallace, B. A. (2008) Protein secondary structure analyses from circular dichroism spectroscopy: methods and reference databases. *Biopolymers* **89,** 392–400
50. Diallo, A., Barrett, T., Barbron, M., Meyer, G., and Lefèvre, P. C. (1994) Cloning of the nucleocapsid protein gene of peste-des-petits-ruminants virus: relationship to other morbilliviruses. *J. Gen. Virol.* **75,** 233–237
51. Zhang, X., Bourhis, J. M., Longhi, S., Carsillo, T., Buccellato, M., Morin, B., Canard, B., and Oglesbee, M. (2005) Hsp72 recognizes a P binding motif in the measles virus N protein C-terminus. *Virology* **337,** 162–174
52. Radecke, F., Spielhofer, P., Schneider, H., Kaelin, K., Huber, M., Dötsch, C., Christiansen, G., and Billeter, M. A. (1995) Rescue of measles viruses from cloned DNA. *EMBO J.* **14,** 5773–5784
53. Plumet, S., and Gerlier, D. (2005) Optimized SYBR Green real-time PCR assay to quantify the absolute copy number of measles virus RNAs using gene specific primers. *J. Virol. Methods* **128,** 79–87
54. Vincent, S., Spehner, D., Manié, S., Delorme, R., Drillien, R., and Gerlier, D. (1999) Inefficient measles virus budding in murine L.CD46 fibroblasts. *Virology* **265,** 185–195
55. Tompa, P. (2002) Intrinsically unstructured proteins. *Trends Biochem. Sci.* **27,** 527–533
56. Iakoucheva, L. M., Kimzey, A. L., Masselon, C. D., Smith, R. D., Dunker, A. K., and Ackerman, E. J. (2001) Aberrant mobility phenomena of the DNA repair protein XPA. *Protein Sci.* **10,** 1353–1362
57. Dunker, A. K., and Obradovic, Z. (2001) The protein trinity-linking function and disorder. *Nat. Biotechnol.* **19,** 805–806
58. Uversky, V. N. (2002) Natively unfolded proteins: a point where biology waits for physics. *Protein Sci.* **11,** 739–756
59. Uversky, V. N. (2003) Protein folding revisited. A polypeptide chain at the folding-misfolding-nonfolding cross-roads: which way to go? *Cell. Mol. Life Sci.* **60,** 1852–1871
60. Radivojac, P., Iakoucheva, L. M., Oldfield, C. J., Obradovic, Z., Uversky, V. N., and Dunker, A. K. (2007) Intrinsic disorder and functional proteomics. *Biophys. J.* **92,** 1439–1456
61. Freyer, M. W., and Lewis, E. A. (2008) Isothermal titration calorimetry: experimental design, data analysis, and probing macromolecule/ligand binding and kinetic interactions. *Methods Cell Biol.* **84,** 79–113
62. Bryson, K., McGuffin, L. J., Marsden, R. L., Ward, J. J., Sodhi, J. S., and Jones, D. T. (2005) Protein structure prediction servers at University College London. *Nucleic Acids Res.* **33,** W36–W38
63. McGuffin, L. J., Bryson, K., and Jones, D. T. (2000) The PSIPRED protein structure prediction server. *Bioinformatics* **16,** 404–405
64. Tell, G., Perrone, L., Fabbro, D., Pellizzari, L., Pucillo, C., De Felice, M., Acquaviva, R., Formisano, S., and Damante, G. (1998) Structural and functional properties of the N transcriptional activation domain of thyroid transcription factor-1: similarities with the acidic activation domains. *Biochem. J.* **329,** 395–403
65. Hua, Q. X., Jia, W. H., Bullock, B. P., Habener, J. F., and Weiss, M. A. (1998) Transcriptional activator-coactivator recognition: nascent folding of a kinase-inducible transactivation domain predicts its structure on coactivator binding. *Biochemistry* **37,** 5858–5866
66. Dahlman-Wright, K., and McEwan, I. J. (1996) Structural studies of mutant glucocorticoid receptor transactivation domains establish a link between transactivation activity *in vivo* and α-helix-forming potential *in vitro*. *Biochemistry* **35,** 1323–1327
67. Yegambaram, K., and Kingston, R. L. (2010) The feet of the measles virus polymerase bind the viral nucleocapsid protein at a single site. *Protein Sci.* **19,** 893–899
68. Blocquel, D., Habchi, J., Gruet, A., Blangy, S., and Longhi, S. (2012) Compaction and binding properties of the intrinsically disordered C-terminal domain of Henipavirus nucleoprotein as unveiled by deletion studies. *Mol. Biosyst.* **8,** 392–410
69. Uversky, V. N. (2011) Intrinsically disordered proteins may escape unwanted interactions via functional misfolding. *Biochim. Biophys. Acta* **1814,** 693–712

70. Houben, K., Marion, D., Tarbouriech, N., Ruigrok, R. W., and Blanchard, L. (2007) Interaction of the C-terminal domains of Sendai virus N and P proteins: comparison of polymerase-nucleocapsid interactions within the paramyxovirus family. *J. Virol.* **81,** 6807–6816
71. Rager, M., Vongpunsawad, S., Duprex, W. P., and Cattaneo, R. (2002) Polyploid measles virus with hexameric genome length. *EMBO J.* **21,** 2364–2372
72. Liljeroos, L., Huiskonen, J. T., Ora, A., Susi, P., and Butcher, S. J. (2011) Electron cryotomography of measles virus reveals how matrix protein coats the ribonucleocapsid within intact virions. *Proc. Natl. Acad. Sci. U.S.A.* **108,** 18085–18090
73. Hirano, A., Ayata, M., Wang, A. H., and Wong, T. C. (1993) Functional analysis of matrix proteins expressed from cloned genes of measles virus variants that cause subacute sclerosing panencephalitis reveals a common defect in nucleocapsid binding. *J. Virol.* **67,** 1848–1853
74. Vincent, S., Gerlier, D., and Manié, S. N. (2000) Measles virus assembly within membrane rafts. *J. Virol.* **74,** 9911–9915
75. Riedl, P., Moll, M., Klenk, H. D., and Maisner, A. (2002) Measles virus matrix protein is not cotransported with the viral glycoproteins but requires virus infection for efficient surface targeting. *Virus Res.* **83,** 1–12
76. Cathomen, T., Mrkic, B., Spehner, D., Drillien, R., Naef, R., Pavlovic, J., Aguzzi, A., Billeter, M. A., and Cattaneo, R. (1998) A matrix-less measles virus is infectious and elicits extensive cell fusion: consequences for propagation in the brain. *EMBO J.* **17,** 3899–3908
77. Suryanarayana, K., Baczko, K., ter Meulen, V., and Wagner, R. R. (1994) Transcription inhibition and other properties of matrix proteins expressed by M genes cloned from measles viruses and diseased human brain tissue. *J. Virol.* **68,** 1532–1543
78. Iwasaki, M., Takeda, M., Shirogane, Y., Nakatsu, Y., Nakamura, T., and Yanagi, Y. (2009) The matrix protein of measles virus regulates viral RNA synthesis and assembly by interacting with the nucleocapsid protein. *J. Virol.* **83,** 10374–10383
79. Brown, H. R., Goller, N., Thormar, H., and Norrby, E. (1987) Fuzzy material surrounding measles virus nucleocapsids identified as matrix protein. Brief report. *Arch. Virol.* **94,** 163–168
80. Dubois-Dalcq, M., and Barbosa, L. H. (1973) Immunoperoxidase stain of measles antigen in tissue culture. *J. Virol.* **12,** 909–918
81. Robbins, S. J., Bussell, R. H., and Rapp, F. (1980) Isolation and partial characterization of two forms of cytoplasmic nucleocapsids from measles virus-infected cells. *J. Gen. Virol.* **47,** 301–310